Oblique rifting triggered by slab tearing : the case of the Alboran rifted margin in the eastern Betics

Marine Larrey[1,2], Frédéric Mouthereau[1*], Damien Do Couto[3], Emmanuel Masini[4], Anthony Jourdon[5], Sylvain Calassou[2] and Véronique Miegebielle[2]

[1]Université Paul Sabatier, Géosciences Environnement Toulouse, GET UMR 5563, Toulouse, France.

[2]TOTAL S.A., Centre Scientifique & Technique Jean Féger, Pau, France.

[3]Sorbonne Université, CNRS-INSU, Institut des Sciences de la Terre Paris, ISTeP UMR 7193, F-75005 Paris, France.

[4]M&U sas, France.

[5]Institute of Geophysics, Ludwig-Maximilians-Universität München, Munich, Germany.

Corresponding author: Frédéric Mouthereau (frederic.mouthereau@get.omp.eu)

Abstract

The tectonic evolution of highly oblique continental margins that result from back-arc extension above lithospheric STEP faults is poorly understood. Here, we investigate the case of the Alboran margin in the eastern Betics characterized by crustal thinning of 15-10 km, oblique to the direction of slab retreat. The current deformation patterns indicate that oblique back-arc rifting is underway. However, it is unclear whether these conditions are those that prevailed during the formation of the metamorphic domes and intramontane basins. We review the temporal and spatial evolution of Neogene sedimentary basins and brittle deformation in the eastern Betics, and exploit offshore seismic reflection lines to propose a crustal-scale section across the oblique margin. The history of sediment infill and rates of subsidence combined with the analyses of fault slip data, confirms that brittle extension oriented from N20°E to EW occurred during an interval spanning from the Serravallian-early Tortonian to the late Tortonian (14-8 Ma). This extension is associated with both normal and strike-slip regimes and the evolution of the strike-slip fault zones flanking the metamorphic domes. The transtensional model forms a coherent scheme linking the ductile deformation associated with metamorphic domes and the formation of EW- and NW-SE/NNW-SSE-directed sedimentary basins in the brittle upper crust during the Tortonian. The oblique extension, which is closely associated with STEP faulting, occurred during the regional convergence between Africa and Iberia since the Miocene. Only recently, around 8 Ma, slab detachment started to migrate westward, leading to tectonic inversion in the eastern Betics. Such a type of narrow oblique rifted margin associated with transform-like plate boundaries is not unique but is expected to be hardly preserved in the geological record due to the transient nature of retreating subduction systems.

1 Tear faulting and the formation of oblique rifted margin in the Betics

Lithospheric tear faults or subduction-transform edge propagator (STEP) faults are propagating strike-slip faults that accommodate the differential motion between the retreating subduction zone and the overriding back-arc plate (Govers and Wortel, 2005). Because of the relative motion between back-arc and surrounding plates, they are also propagating strike-slip faults defined by a sharp contrast in crustal thickness. As noted by Govers and Wortel (2005) such oblique fault boundaries do not necessarily form proper transform plate boundaries but broad zones of distributed deformation, accommodating differential trench-parallel extension, strike-slip motion and rotation. In case the lithospheric tear propagates within the continent-ocean transition, a narrow continental margin forms highly oblique to the direction of back-arc extension. This is documented, for instance, in the Carribean, along the transcurrent Carribean-South America plate boundary (Pindell and Kennan, 2009) or on the margin of the South Orckney microcontinent, along the Scotia-Antarctic plate boundary (Dalziel et al., 2013). Despite the large-scale kinematic picture is relatively well understood, there are only few places on Earth where continental crustal deformation associated with slab-edge continental rift system can be studied both onland and offshore.

Here, we focus on the eastern Betic Cordillera, which constitutes a rifted margin defined by decreasing crustal thickness from >35 km to 20 km (Diaz et al., 2016) (**Figs 1 and 2**). This region is seen to develop above a STEP fault at the boundary between the Alboran basin and the Iberian paleomargin (Badji et al., 2014; Gallais et al., 2013; Jolivet et al., 2021a; Mancilla et al., 2015a). The tectonic expression of the transcurrent deformation during crustal extension above the lithospheric tear is however controversial. On the one hand, low-angle ductile extensional detachments with a top-to-the-west sense of shear are the main features accommodating deformation in the overriding plate. Yet, a-type metamorphic domes in the lower crust, elongated parallel to the E-W direction (**Fig. 1**), are viewed to express the transtensional deformation at the tip of propagating tear (Pourhiet et al., 2012). On the other hand, strike-slip faulting is interpreted as a late brittle deformation feature associated with differential E-W crustal extension between the metamorphic domes in the eastern Betics (Alpujarras fault zone ; Sanz de Galdeano and Vera, 1992; Sanz de Galdeano et al., 1985; Martínez-Martínez et al., 2006) and in the western Betics (e.g. Torcal fault zone ; Frasca et al., 2016 ;) unrelated to ductile deformation (**Fig. 1**). In line with the latter interpretation, the dextral motion these strike-slip transfer faults accommodate is assumed to be modest, reflecting a recent post-8 Ma kinematic change that accompanies the stalling of westward slab rollback, the onset of tectonic inversion in the Gibraltar Arc (Do Couto et al., 2014; d'Acremont et al., 2020; Jolivet et al., 2021a; Martínez-García et al., 2017), and progressive slab tearing and delamination of the lithospheric mantle from the eastern to the central Betics (Mancilla et al., 2015a ; García-Castellanos and Villaseñor, 2011; Spakman et al., 2018).

The lack of structural, temporal constraints and quantification of belt-parallel motion along these faults indicates, however, that we do not yet fully understand their link with the long-term evolution of slab tearing   and margin formation. For instance, the current deformation patterns in the Central Betics, where metamorphic domes are present, brings evidence that both strike-slip faulting and extension operate synchronously. This is shown by the west-directed GPS velocities increasing westwards indicating ongoing extension, and the west-directed displacements increasing from North to South, towards the Alboran domain, revealing right-lateral shear (**Fig. 2**). The current transtensional deformation across the Betic Cordillera is consistent with the current stress regime defined by extension

direction highly oblique (max. 20°) to the Betic structural trend (or 70° spanned by the direction of extension and normal of the rift trend). Right-lateral transtensional deformation further agrees with the extrusion model of the Alboran basin towards the Gibraltar arc to the West (Borque et al., 2019; Palano et al., 2015) as a consequence of indentation by the east Abloran domain likely enhanced by resistance slab dragging (Spakman et al., 2018). In the East, the extrusion is accommodated by left-lateral strike-slip displacement along the Eastern Betic Shear Zone (EBSZ; Borque et al., 2019), shaped by the Carboneras Fault (CF) and Palomares Fault (PF), which separates the extrusion domain were extension and transtension is prevailing from the Águilas Arc where N-S indentation is well documented (Ercilla et al., 2022). This fault extends offshore, across the Alboran Sea, in the larger Trans-Alboran Shear Zone (De Larouzière et al., 1988; Stich et al., 2006) moving at ~4 mm/yr, equivalent to the regional 5 mm/yr NW-directed convergence between Africa (Nubia) and Europe (**Fig. 2**; Echeverria et al., 2013; Koulali et al., 2011; Nocquet, 2012; Palano et al., 2015, 2013; Vernant et al., 2010). Here, we hypothesize that the present-day oblique extension patterns is at play since the Miocene and explain the formation of the narrow Alboran rifted margin.

Coordinate System: WGS 1984 UTM Zone 30N, Projection: Transverse Mercator
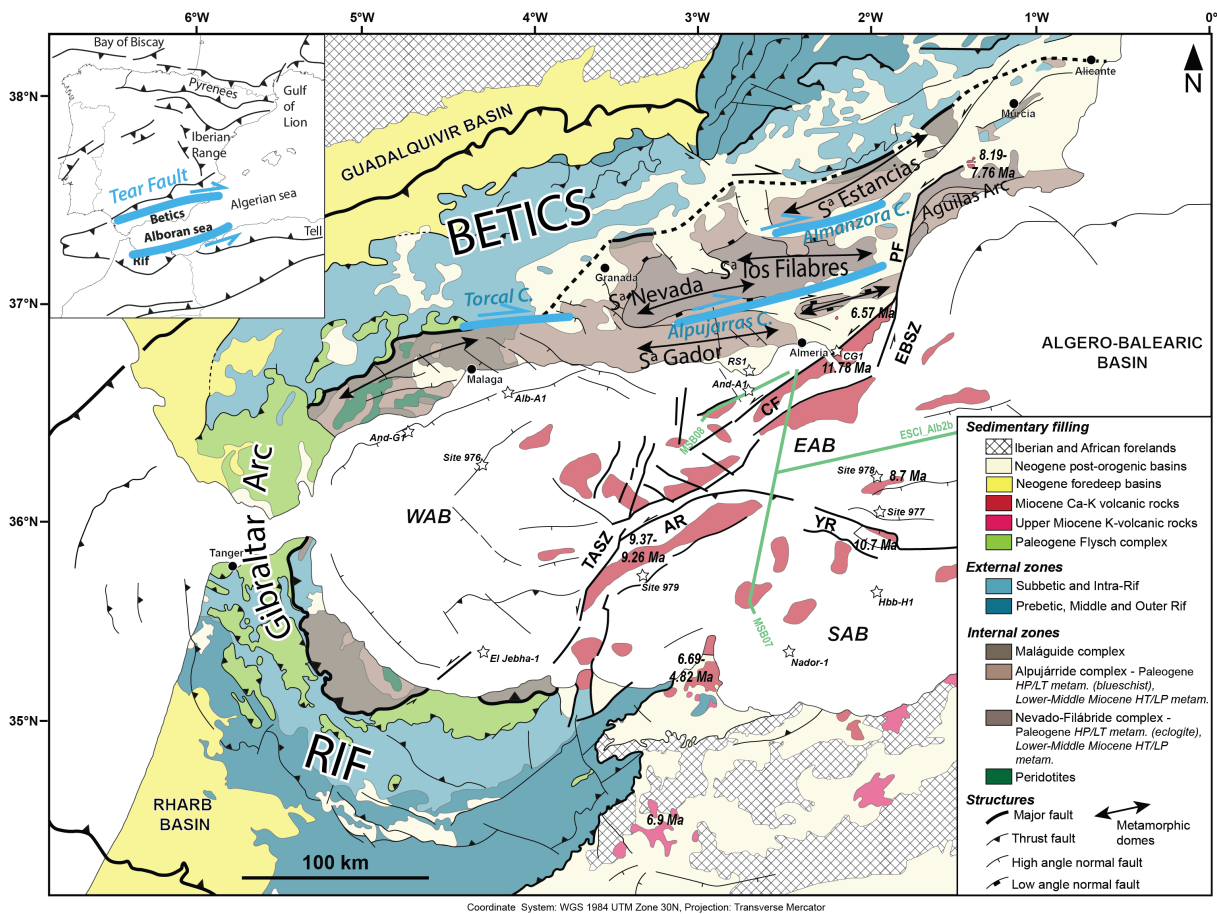
Figure 1 : Geological map of the Betic-Rif arc. Main tectonic units and age of volcanism as well as major structures and Neogene sedimentary basins are shown. The studied offshore seismic lines (red) is displayed as well as offshore wells and ODP sites (★) for stratigraphic calibration in the East (EAB), South (SAB) and West Alboran basins (WAB). CF: Carboneras Fault; PF : Palomares Fault; AR: Alboran Ridge; YR: Yusuf Ridge; EBSZ : East Betic Shear Zone; TASZ: Trans-Alboran Shear Zone.

Only recently high-resolution 3D numerical models have been able to predict the deep structure of oblique rift domains. These models can be used as a guide to re-evaluate the evolution of the Betics. 3D models by Jourdon et al. (2021) predict that oblique extension results in narrow rifted margins, strike-slip faults and corridors coupled with subsident pull-apart basins, normal faults and block rotations (**Fig. 3**). The recognition of block rotation in the Betic arc (Crespo-Blanc et al., 2016; Platzman, 1992), strike-slip fault zones (**Fig. 1**) and NW-SE normal faulting, which defines extension direction highly oblique to the margin (Galindo-Zaldivar et al., 2003; **Figs 1 and 2**), support this view. The simulations also show that the deeper ductile crust experiences thinning (vertical flattening) and stretching perpendicular to the strike of the margin in accordance with stretching lineations parallel to the metamorphic domes and low-angle detachments (**Fig. 3**). Other types of 3D numerical experiments show that sediment loading of strike-slip faults can result in assymetric flexural basin with apparent normal fault throw (Neuharth et al., 2021) that can be mistakenly interpreted as resulting from orthogonal extension. Asymmetric basins are indeed intriguing characteristics of intramontane basins in the Betics (Rodríguez-Fernández et al., 2011; Augier et al., 2013; Do Couto et al., 2014 ; Giaconia et al., 2014). Although primarily found associated with divergent plate boundaries e.g. in the Gulf of California (Fossen et al., 2013; Fossen and Tikoff, 1998) highly oblique extension is also documented in active transform regions along the San Andreas Fault (Teyssier and Tikoff, 1998) or the North Anatolian Fault in Marmara Sea (Okay et al., 2004). A detailed analysis of highly oblique rifting deformation in the Gulf of California recognises similar tectonic elements as for the Betics, such as extensional detachment systems orthogonal to the divergence and upper crustal folds trending parallel to the divergence (Fossen et al., 2013).
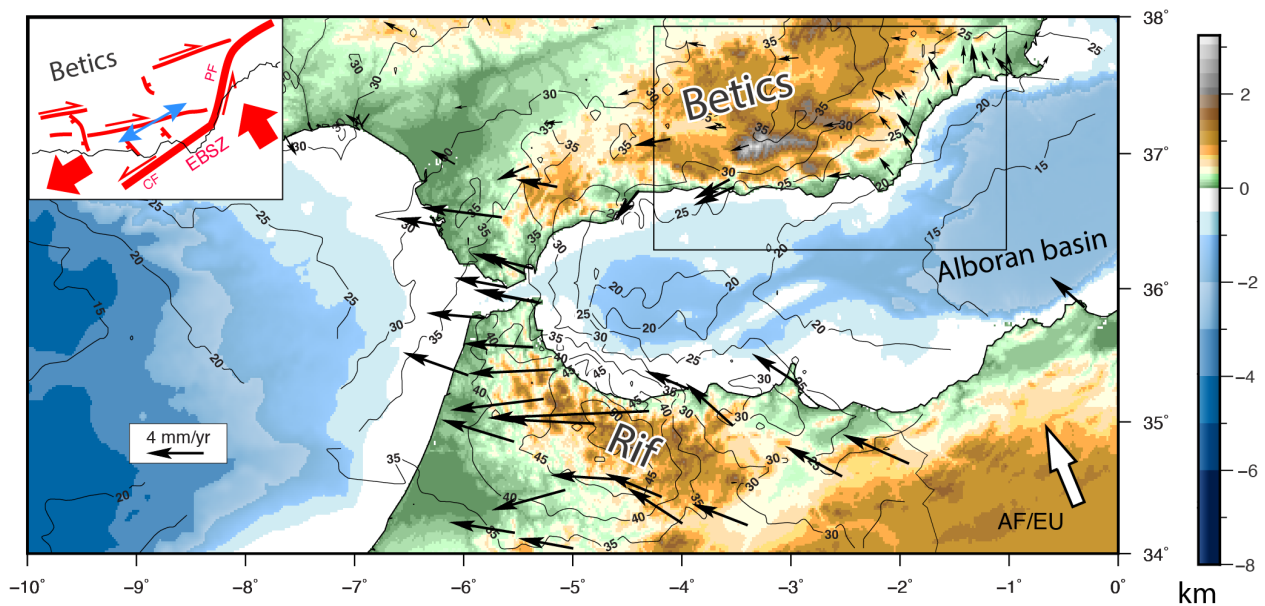
Figure 2 : Present-day kinematics in the Betic-Rif arc and eastern Betic Cordillera (inset). GNSS-based displacements in the western Alboran block and north-western Africa shown in a fixed Eurasian reference frame (black arrows after

110 Palano et al., 2015) are oblique to the AF/EU plate convergence (white arrow) inferred from plate tectonic Morvel
111 model (Argus et al., 2011). Labelled contours depict the crustal depth given in kilometers as inferred from deep seismic
112 profiles and receiver functions analysis (Diaz et al., 2016). In the eastern Betic (inset), W-directed stretching is taken
113 up by EW-directed right-lateral strike-slip fault and NW-SE normal faults. Extension direction resolved from focal
114 mechanisms (blue arrows) are after (Stich et al., 2006). CF: Carboneras Fault; PF : Palomares Fault; AR: Alboran
115 Ridge; YR: Yusuf Ridge; EBSZ : East Betic Shear Zone; TASZ: Trans-Alboran Shear Zone.
116

117 Several tectonic features need further discussion however. First, the relevance of strike-slip faulting in the past is

118 debatable as only a few occurrence of crustal-scale strike-slip faults are mapped. Second, the detail of the temporal

119 and spatial relationships between the formation of the oblique/transform margin and STEP faulting remain elusive.

120 We here review the temporal and spatial evolution of Neogene intramontane sedimentary basins and related brittle

121 deformation in the eastern Betics. In addition, we exploit offshore seismic reflection lines to propose a new crustal-

122 scale section across the oblique margin. Based on these constraints we present a tectonic scenario for the formation of

123 the high-obliquity rifted margin controlled by STEP faulting.

124
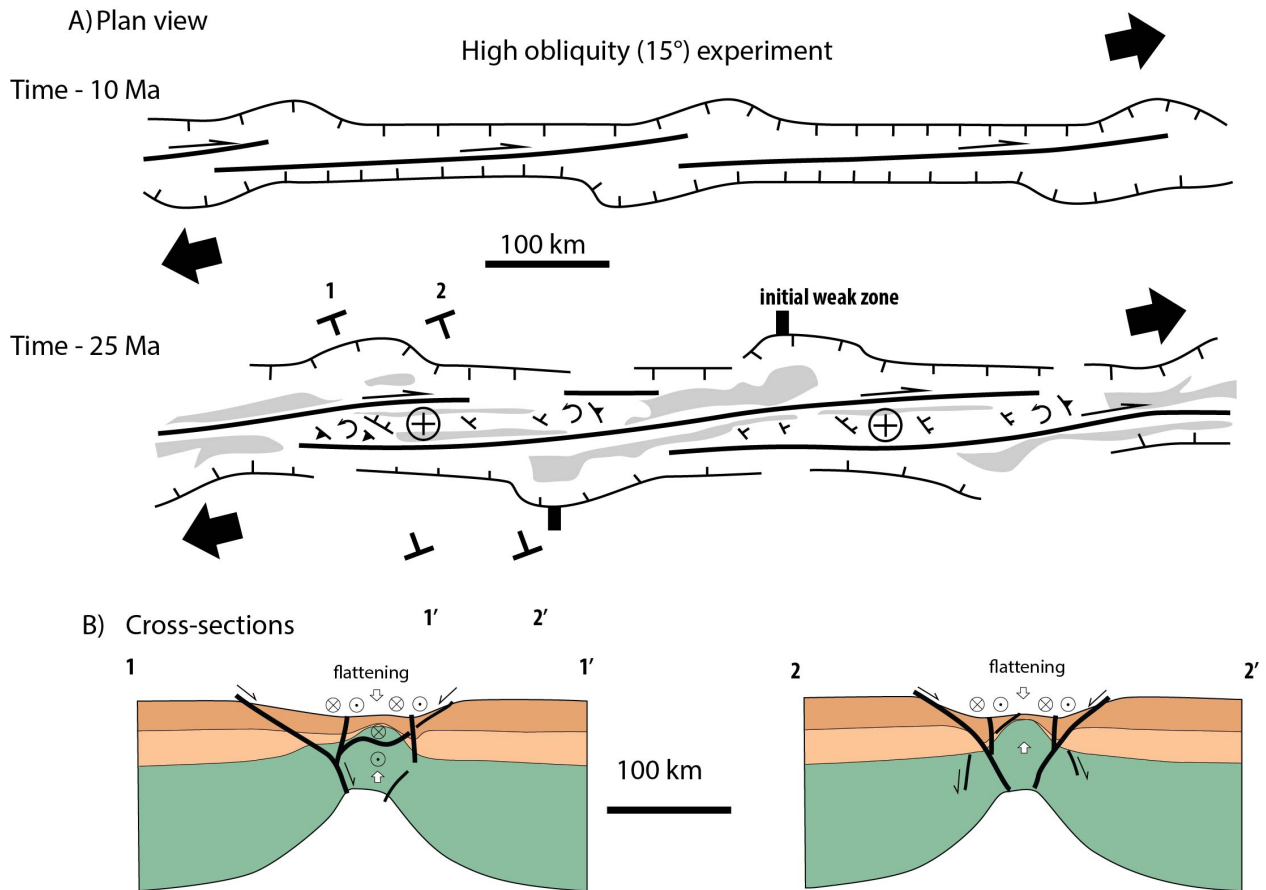
125

126 **Figure 3** : Sketch showing two steps (after 10 Myrs and 24 Myrs) of a 3D thermo-mechanical model of oblique rifting
127 in plan view (A) and cross-sections (B). Results are redrawn after (Jourdon et al., 2021) for the case of a highly oblique
128 experiment where extension is set with an angle of 15° with respect to the rift axis. Grey regions in (A) are basins
129 adjacent to uplifted domains (cross-circle symbol) associated with right-lateral strike-slip faults. Cross-sections (B)
130 depict the abrupt crustal thinning that occur perpendicular. Crustal thining is most visible for the lower crust and
131 produces the formation of an abrupt necking domain controlled by rift-parallel normal faults dipping towards the
132 center of the rift and right-lateral strike-slip faults.

133

2. Geodynamics and STEP faulting in the Betics

The onset of N-directed movement of Africa, by the Late Cretaceous-Paleogene, led to far-field, Laramide-like contraction from Morocco throughout Western Europe (Mouthereau et al., 2021). South of Iberia, in the Betic-Rif domain, the closure of hyper-extended rift systems and oceanic basins of the Atlantic-Alpine Tethys resulted in the development of a proto-Betic accretionary prism, likely largely submerged (Angrand and Mouthereau, 2021; Daudet et al., 2020; Vergés and Fernàndez, 2012). By about 50 Ma, the acceleration of plate convergence led to the shortening of continental rift and oceanic basins and topographic uplift all over Iberia (Daudet et al., 2020; Mouthereau et al., 2021, 2014; Rat et al., 2019; Vacherat et al., 2016; Waldner et al., 2021) associated with onset of continental rifting along the Western European Rift (e.g. Mouthereau et al., 2021). 35 Ma ago, as Africa convergence slowed down, the western Mediterranean sea opened accompanied by retreating slabs (Dewey, 1988; Dewey et al., 1989; Faccenna et al., 2014; Jolivet and Faccenna, 2000; Rosenbaum et al., 2002). Subduction occurred mainly before 30 Ma as argued by age constraints on high-pressure mineral assemblages (Augier et al., 2005a; Bessière et al., 2021; Booth-Rea et al., 2015; Gomez-Pugnaire and Fernandez-Soler, 1987; Platt and Vissers, 1989; Platt and Whitehouse, 1999) and has been suggested to last until the mid-Miocene in the eastern Betics e.g. (Platt et al., 2013). The timing of formation of the Alboran basin is constrained to 23 to 16 Ma by the oldest deposits found on Alboran basement and by the timing of high-temperature metamorphic overprint and rapid cooling to shallow crustal temperature (Bessière et al., 2021; Daudet et al., 2020; Janowski et al., 2017; Johnson et al., 1997; Platt et al., 2005; Sosson et al., 1998; Vázquez et al., 2011; Zeck et al., 1992). The eastern Alboran basin formed later, mostly by late Miocene arc magmatism (Booth-Rea et al., 2007; 2018; Gómez de la Peña et al., 2020a).

All kinematic reconstructions agree that extension results from the westward migration of the arc front and retreat of the Alboran slab, well imaged below the Gibraltar arc as a steeply-dipping high-velocity anomaly (Bezada et al., 2013; Heit et al., 2017; Mancilla et al., 2018, 2015a, 2015b; Palomeras et al., 2014; Spakman and Wortel, 2004; Villaseñor et al., 2015). These reconstructions, however, differ according to the paleo-position of Alboran terrane, and hence to the amount and vergence of subduction (Angrand and Mouthereau, 2021; Hinsbergen et al., 2014; Lonergan and White, 1997; Romagny et al., 2020; Rosenbaum et al., 2002; Vergés and Fernàndez, 2012). Seismic tomography reveals that slab detachment and tearing occur along the conjugate Alboran margins of the southern Betics and northern Africa (Govers and Wortel, 2005; Heit et al., 2017; Mancilla et al., 2015a; Meighan et al., 2013; Spakman and Wortel, 2004).

In **Fig. 4** we refer to the reconstruction of Angrand and Mouthereau (2021) that has the advantage of reconciling previous western Mediterranean models (Romagny et al., 2020; Vergés & Fernàndez, 2012) with recent thermochronological analyses in western Betics (Daudet et al., 2020) and other geological data (see compilation in Mouthereau et al., 2021). This model considers that the Alboran domain has been rifted from Iberia during the Jurassic. It is in agreement with detrital and igneous zircon U-Pb ages that suggest Alboran was attached to Iberia in the late Paleozoic (Jabaloy-Sánchez et al, 2021). It also accounts for the existence of an upper Cretaceous-Paleogene foreland basin that formed adjacent to a proto-Betic orogen and in continuity eastwards with the Balearic Promontory. In that

169 respect, it contrasts with other models placing the Alboran domain to the south of the Balearic Promontory (Moragues
170 et al., 2021; van Hinsbergen et al., 2014).
171 In this reconstruction about 400 km of slab retreat is estimated since about 35 Ma (gray path, blue arrows in **Fig. 4**).
172 It is worth noting that for Romagny et al. (2020) a similar amount (i.e. 400 km) is accommodated by back-arc extension
173 of the Alboran crust, implying the same magnitude of displacement along the STEP fault in the Betics. In the
174 reconstruction of Angrand and Mouthereau (2021), however, crustal thinning in Alboran basin is linked to
175 delamination retreat of the Alboran lithospheric mantle towards the west. Because of the decoupling between crust
176 and mantle, the length of the delaminated slab resolved at depth in seismic tomography, should not be simply translated
177 into the amount of E-W crustal extension in the Alboran domain. This further implies that the displacement across the
178 STEP fault must be also less than 400 km. Daudet et al. (2020) suggested that an extension of 110 km estimated from
179 the restoration of low-angle detachment systems in the central and eastern Betics (Martínez-Martínez et al., 2002) is
180 likely to be a more accurate crustal estimate of the movement Alboran domain rather than the total slab length.
181
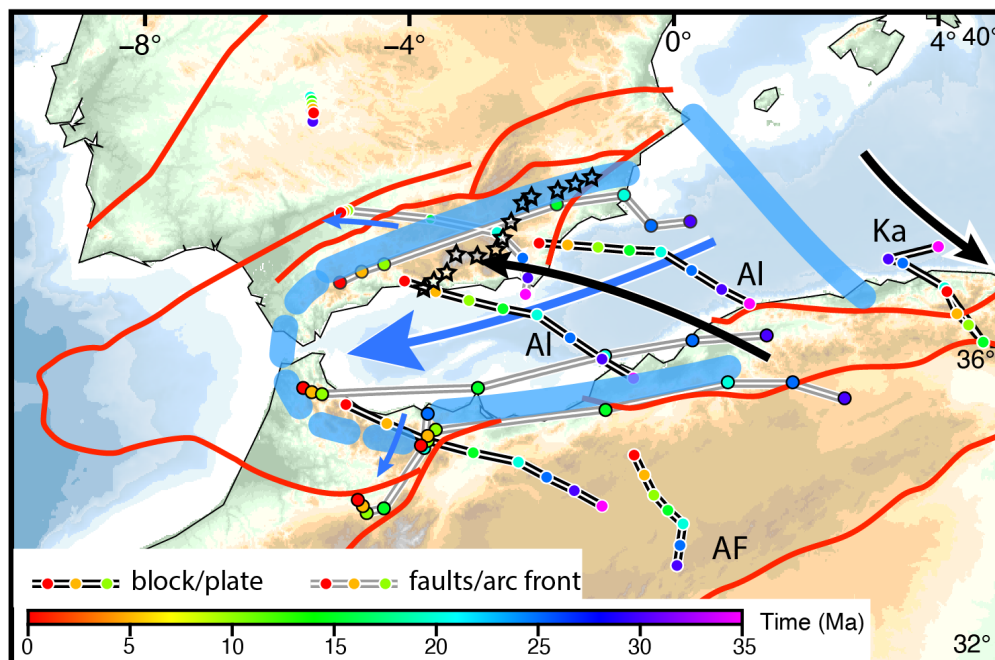
182
183 **Figure 4**: Kinematics of African plate (AF), Alboran (Al) and Kabylides (Ka) blocks with respect to fixed European
184 plate since 35 Ma reconstructed after Angrand and Mouthereau (2021). Thick blue lines depicts the approximate
185 position of lithospheric tear faults (between Al and Europe and Africa) and transfer faults (between Al and Ka). Tear
186 faults located in Betics and Rif are after Jolivet et al. (2021b). Black stars depicts the positioned of tear fault in the
187 Betics as defined by Mancilla et al. (2015a). Black arrows indicate the movement of Al and Ka with respect to Europe
188 along black motion paths presented from 35 Ma to present. Grey motion paths refer to the motion of specific structures
189 relative to Europe, including the motion of the arc front (thick blue dashed line) and faults in red. Dark blue arrow
190 depicts the movement of the arc front due to retreating delamination towards the west.
191

3. Miocene extension in the eastern Betics

3.1 Relationships between domes and basins : from transtension and pure extension to late tectonic inversion

194 The most prominent extensional features in the eastern Betics are : 1) E-W elongated ranges that formed metamorphic
195 domes with foliations bearing prominent E-W stretching lineations, for instance, in the Nevado-Filabrides
196 Complex (**Fig. 5**; e.g. Sierra de los Filabres, Sierra Nevada, and the Sierra de las Estancias) and Serravallian-Tortonian
197 sedimentary basins (Tabernas-Sorbas, Alpujarras, Almanzora and Huércal-Overa basins); 2) NNW-SSE/NW-SE
198 normal fault systems and basins oblique to the domes such as the NW-SE trending Guadix-Baza and Alhabia basins
199 (Galindo-Zaldivar et al., 2003; Martínez-Martínez and Azañón, 1997) (**Fig. 5**). They are described as asymmetric half
200 grabens (Do Couto et al., 2014; Martínez-Martos et al., 2017; Pedrera et al., 2010, 2009) formed during the Upper
201 Serravallian-Early Tortonian (Augier et al., 2005b; Augier et al., 2013; Meijninger and Vissers, 2006). Several of
202 these NW-SE faults are active and cut across the metamorphic domes and the sedimentary basins (Augier et al., 2005a;
203 Booth-Rea et al., 2004; Giaconia et al., 2012; Montenat and Ott d'Estevou, 1999).

204 In addition to these structures, there are E-W right-lateral strike-slip fault zones and parallel depressions, like the
205 Alpujarras fault zone between the Sierra de Gádor and the Sierra Nevada, and the Almanzora fault zone between the
206 Sierra de los Filabres and Sierra de las Estancias (**Fig. 5**). The left-lateral Carboneras and Palomares fault system
207 (Reicherter and Hübscher, 2006; Scotney et al., 2000) marks the tectonic limit with the Cabo de Gata volcanic province
208 (**Fig. 5**).

209 The domes are extension-related features interpreted either as 1) EW-metamorphic domes resulting from the
210 exhumation in the footwall of a regional W-directed extensional low-angle detachments, later folded during post-
211 Tortonian N-S contraction (e.g. Montenat & Ott d'Estevou, 1990; Sanz de Galdeano and Vera, 1992; Sanz de
212 Galdeano and Alfaro, 2004; Martínez-Martínez et al., 2002; Martínez-Martos et al., 2017; Pedrera et al., 2010, 2007)
213 or 2) Miocene metamorphic domes formed by constrictional ductile strain regime accompaniying W-directed
214 stretching of the Alboran domain and trench retreat, with limited overprint by the Tortonian contraction ca. 8 Ma
215 (Augier et al., 2013; Augier et al., 2005; Augier et al., 2005b; Galindo-Zaldivar et al., 2015; Jolivet et al., 2021b;
216 Martínez-Martínez et al., 2002). Low-temperature constraints from the Nevado-Filabride and Alpujarride complexes
217 confirm the west-directed exhumation of the basement that occurred progressively from the Sierra de los Filabres at
218 ~13-11 Ma (Serravallian) in the East to the Sierra Nevada at 8-6 Ma (Tortonian) in the West (Clark and Dempster,
219 2009; Janowski et al., 2017; Johnson et al., 1997; Platt et al., 2005; Reinhardt et al., 2007; Vázquez et al., 2011).

220
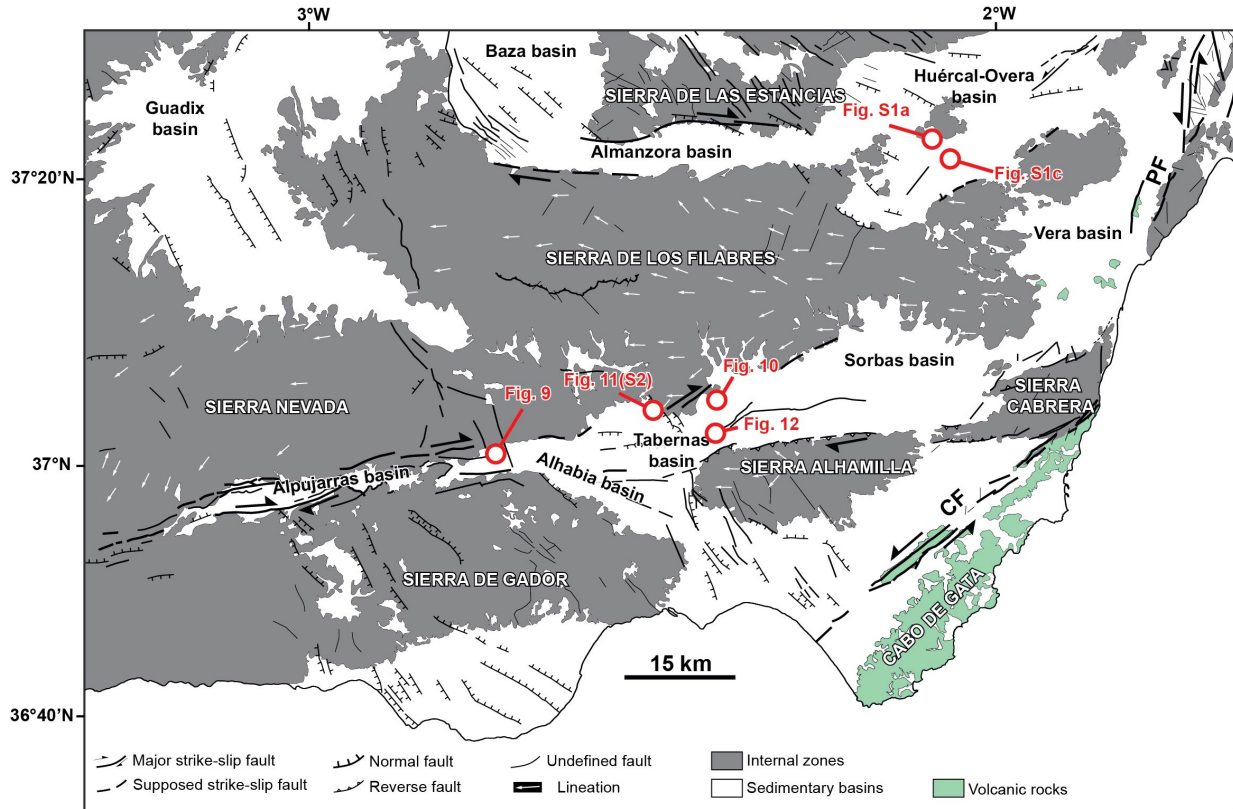
Figure 5 : Tectonic map of the eastern Betics showing the main structural elements in black after Augier et al. (2005) and Do Couto (2014). CF: Carboneras Fault; PF : Palomares Fault.

Tectonic models for the formation of Neogene intramontane sedimentary basins vary depending on the prevailing tectonic regime. EW-directed basins have been early described as pull-apart basins (e.g Alpujarran fault zone; Sanz de Galdeano et al., 1985). Structural analyses then led to re-interpret these structures as transfer zones resulting from differential extension between exhuming core-complexes (and detachment systems) since the Serravallian (13-11 Ma) later refolded during Tortonian (9-8 Ma) compression in the Eastern Betics while extension is still active in the Central Betics (Martínez-Martínez et al., 2006). Other authors proposed that NE-SW extension lasted until 7.5-7 Ma in the Eastern Betics (Booth-Rea et al., 2004; Giaconia et al., 2014).

In support to the compressional stress regime in the Eastern Betics, Martínez-Martos et al. (2017) interpreted the E-W depressions are related to the tectonic reactivation of crustal weakness zone as dextral strike-slip faults in a counterclockwise rotation, accommodating part of the the N-S shortening. There are evidence that at the end of the Tortonian a regional uplift occurred, rising the remnants of late Tortonian marine platform, 7.2 Ma in age, to 1600 m above sea level in the Sierra de Gádor (Braga et al., 2003; Janowski et al., 2017), coincidently with the onset of contraction in the Sierra Alhamilla and Sierra de los Filabres (e.g. Do Couto et al., 2014), in the Alboran domain (e.g. Martínez-García et al., 2017) and on the margins of the eastern Betic (Giaconia et al., 2013). In addition to shortening, this recent uplift may reflect deep mantle mechanisms like slab tearing or delamination (e.g. Duggen et al., 2003; García-Castellanos and Villaseñor, 2011; Mancilla et al., 2015a).

242   Based on the prevalence in some EW-trending basins, like the Huércal-Overa basin, of EW-trending normal faults,
243   these basins have alternatively been interpreted as resulting from late exhumation stage of the domes, possibly as soon
244   as the Serravallian, but mostly after the early Tortonian (syn-sedimentary faulting) (Augier et al., 2013; Augier et al.,
245   2005b; Meijninger and Vissers, 2006). The NW-SE/NNW-SSE sedimentary basins (Guadix, Baza, Alhabia; **Fig. 5**),
246   in contrast, are extensional basins formed parallel to the direction of the regional compression (Sanz de Galdeano and
247   Vera, 1992; Larouzière et al., 1988). E-W strike-slip fault zones, aligned in the direction of the domes, and NW-SE
248   normal faulting patterns are both key features consistent with predictions from models of oblique extension at
249   transform margin (**Fig. 3**). Yet, based on existing structural and tectonic syntheses a clear temporal relationships
250   between E-W ductile stretching in the domes and transcurrent deformation is not established (**Fig. 5**).
251

3.2 Is the Tortonian rift-related subsidence consistent with oblique extension ?

252
253   The stratigraphic architecture and depositional evolution of Tortonian intramontane basins provides first-order
254   informations on the distribution of crustal thinning. Among the oldest sediments deposited unconformably on the
255   Paleozoic-Triassic basement are the red alluvial conglomerates and deltaic series dated from the Serravallian to the
256   Lower Tortonian (**Fig. 6a**). They are thicker and well exposed on the flanks of the Almanzora basin and on the northern
257   Huércal-Overa basin (HOB), compared to the Alpujarras Corridor (AC) and Tabernas basin (TB) (**Figs. 6 and 7a**;
258   Augier et al., 2013; Pedrera et al., 2010, 2007; Poisson et al., 1996). East of Sorbas basin, it should be noted that
259   Langhian-Serravalian deposits and perhaps sediments as old as Burdigalian have been locally reported (Giaconia et
260   al., 2014).
261   Paleogeographic reconstructions indicate that these Serravallian to Lower Tortonian sediments were deposited on a
262   large emerged domain, stretching from Huercal-Overa to Granada, in the West and in Tabernas, to the South (Braga
263   et al., 2003). Sourced from the Nevado-Filabride metamorphic complex (Hodgson and Haughton, 2004; Kleverlaan,
264   1989; Meijninger and Vissers, 2006; Pedrera et al., 2010, 2007; Pickering et al., 2001; Weijermars et al., 1985) these
265   deposits mark the onset of surface exhumation of the Sierra de Las Estancias and Sierra de Los Filabres.
266   During this intial stage, HOB is the most subsident basin (**Figs. 6b, 7a and 7b**), accumulating sediments at rates of
267   400 m/Ma while rates are 140-180 m/Ma in the Tabernas basin (**Fig. 6b**) (Augier, 2005). Higher subsidence in the
268   HOB, which also started earlier than in other basins, suggests extension occurred originally to the North associated
269   with the exhumation of the Sierra de Las Estancias. Basal continental conglomerates are overlain by grey coarse-
270   grained Tortonian sandstones found occasionally, e.g. in the Almanzora basin, intercalated with marine marls (**Figure
271   6a**). They are topped by mid-Tortonian bioclastic calcarenite and coral reefs (Braga et al., 2003; Martin et al., 1989;
272   Pedrera et al., 2007).
273   During the same interval, TB recorded the deposition of 300 to 400 m of coarse to medium-grained deltaic marine
274   clastics overlying unconformably the lowermost red series (**Fig. 6a**). These sediments pass upwards, e.g. in TB, to
275   deeper marine 1200 m-thick turbiditic and marls series intercalated with regional-scale megabeds, revealing the onset
276   of rapid tectonic subsidence (Haughton, 1994; Kleverlaan, 1989, 1987; Pickering et al., 2001; Weijermars et al., 1985).
277   Details of depositional architecture of the Tortonian suggest that part of this subsidence evolution was controlled by
278   E-W dextral strike-slip faults (Haughton, 2000 ; Baudouy et al., 2021) under transtensional strain.

279 The transition from continental to deep marine sedimentary environments (water depth of 400-600 m according to
280 Poisson et al., 1999) witnesses the rapid rift-related tectonic subsidence achieved during the upper Tortonian times
281 (~9 Ma; **Figs. 6** and **7c**) (Augier et al., 2005b; Montenat and Ott d'Estevou, 1992; Weijermars et al., 1985). At around
282 8 Ma, accumulation rates drop by a factor of two to 200 m/Ma in HOB and 70 m/Ma in TB, revealing a marked
283 reduction in subsidence. Subsidence then became negative as basement uplifted from around 7 Ma (**Figs. 6b** and **7d**)
284 in both TB and HOB.
285
286

287
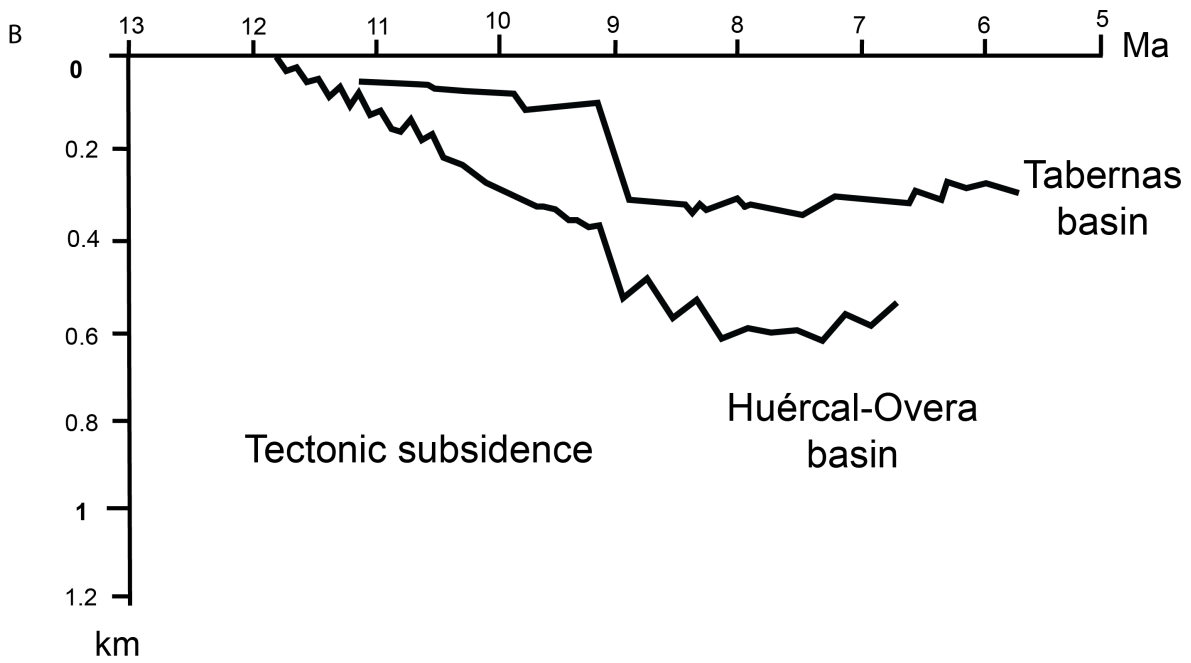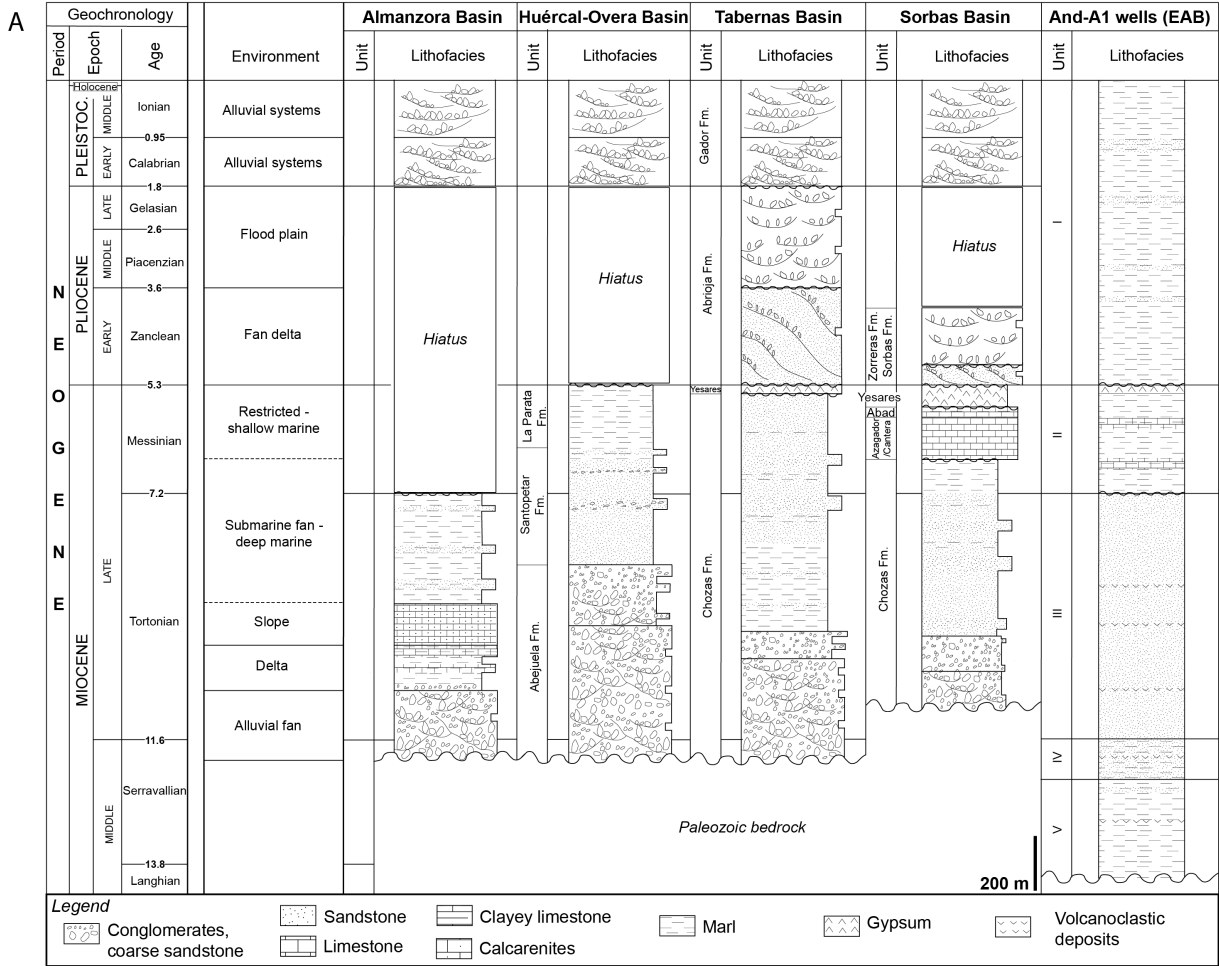
288 **Figure 6** : Stratigraphic evolution and lithologies of intramontane basins in the eastern Betics and offshore A1 well.
289 (a) Neogene stratigraphy and basin-fill correlation in the Almanzora and Huercal-Overa basins (Mora, 1993), Tabernas
290 basin (Hodgson and Haughton, 2004; Kleverlaan, 1989; Pickering et al., 2001) and Sorbas basin (Fortuin and
291 Krijgsman, 2003; Martín and Braga, 1994; Riding et al., 1998). Middle Miocene sedimentary environments in the
292 Alboran Sea are after (Comas et al., 1992). (b) Neogene tectonic subsidence evolution for Tabernas basin and Huércal-
293 Overa basin are from Augier (2004). The curves are obtained from backstripping techniques incorporating eustatic
294 and paleobathymetric corrections.
295

296 The geometry of the Almanzora (Pedrera et al., 2009), Sorbas (e.g. Do Couto et al., 2014) and Huércal-Overa basin

297 basins (Pedrera et al., 2010) inferred from gravity measurements indicate that these basins are asymmetrical and

298 deepening southwards. This sediment infill pattern recalls the formation of asymmetrical basins predicted by

299 numerical models of flexural strike-slip basins (Neuharth et al., 2021). According to this model, the asymmetry

300 observed should reflect the developement of strike-slip basins loaded by sediments originated from the North. In

301 addition, a larger subsidence in HOB is an indication of abrupt crustal thinning to the south of Sierra de las Estancias

302 where the crustal thickness is the largest (**Fig. 2**). Therefore, at least the Serravallian-Tortonian infill patterns agree

303 with oblique extension.

304
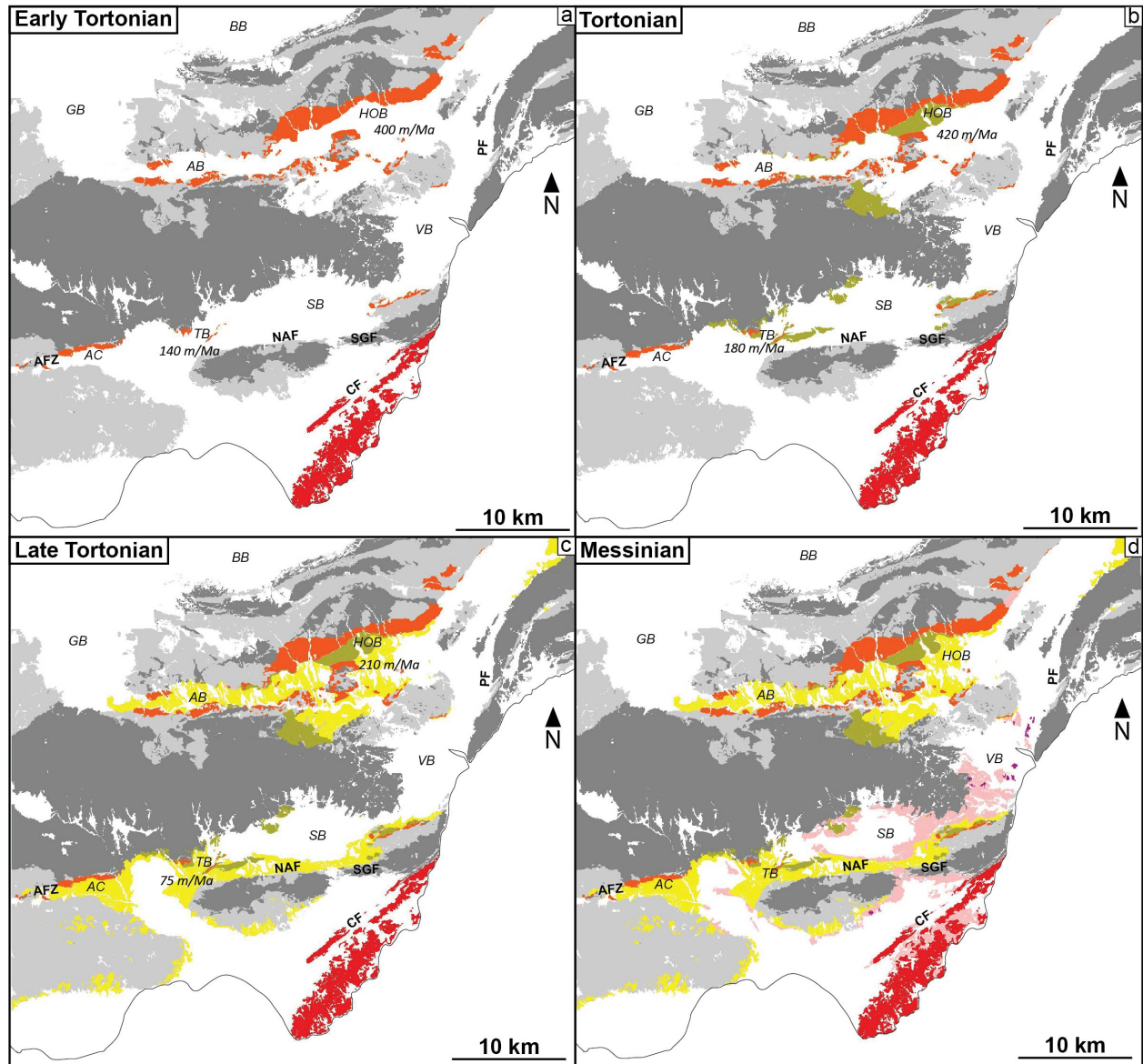
Figure 7: Distribution of (a) lower Tortonian, (b) Tortonian, (c) upper Tortonian and (d) Messinian deposits based on geological mapping of the different basins. CF: Carboneras Fault; PF : P Fault; SGF: South Gafarillo fault; NAF: North Alhamilla fault; AFZ: Alpujarras fault zone; BB: Baza basin; GB: Guadix basin; AB: Almanzora basin; HOB: Huercal-Overa basin; VB: Vera basin; SB: Sorbas basin; TB: Tabernas basin; AC: Alpujarras Corridor.

4. Brittle faulting : pure extension versus transtensional deformation in Neogene basins

4.1. Tectonic regime in the eastern Betics

Figure 8 presents a compilation of 112 fault slip data inversion previously analysed in the eastern Betics combined with new measurements conducted in the Alpujarras Corridor and in the Tabernas basin (**Table S1**). Most faults are syn-Tortonian or cut through the Tortonian. This compilation emphasizes a regional trend of σ3 stress axes oriented

316   NNE-SSW (N20°E) with subbordinate σ3 oriented E-W. In details, this well-defined regional horizontal extension

317   reflects a combination of pure normal faulting regime (σ2 horizontal and oriented NW-SE/WNW-ESE, 73% of stress

318   tensors) and strike-slip faulting regime (σ2 vertical to steeply-dipping and σ1 horizontal an striking NNW-SSE, 27%

319   of stress tensors). N-S to NW-SE compression is also reported in the HOB associated with incipient synform and

320   depocenter which is dated to the lower Tortonian coeval with the prominent EW/WSW-ENE extension (e.g. Pedrera

321   et al., 2010).

322   We describe below, based on a selection of oucrops in the vicinity of the contact between Tortonian basins and major

323   metamorphic domes, the expression of EW and NW-SE extensional faulting in the field. We then discuss how they

324   are linked to the regional stress regimes.

325

326
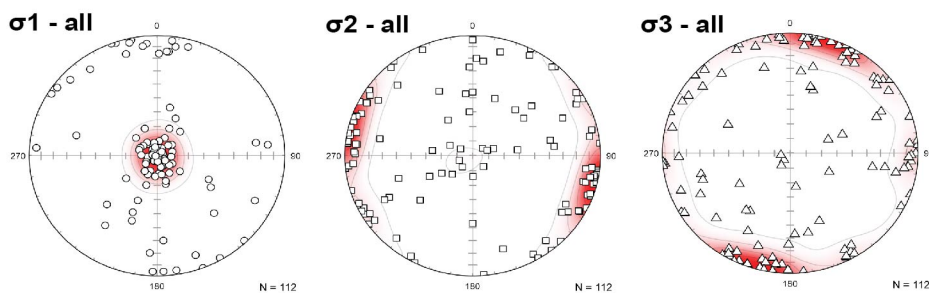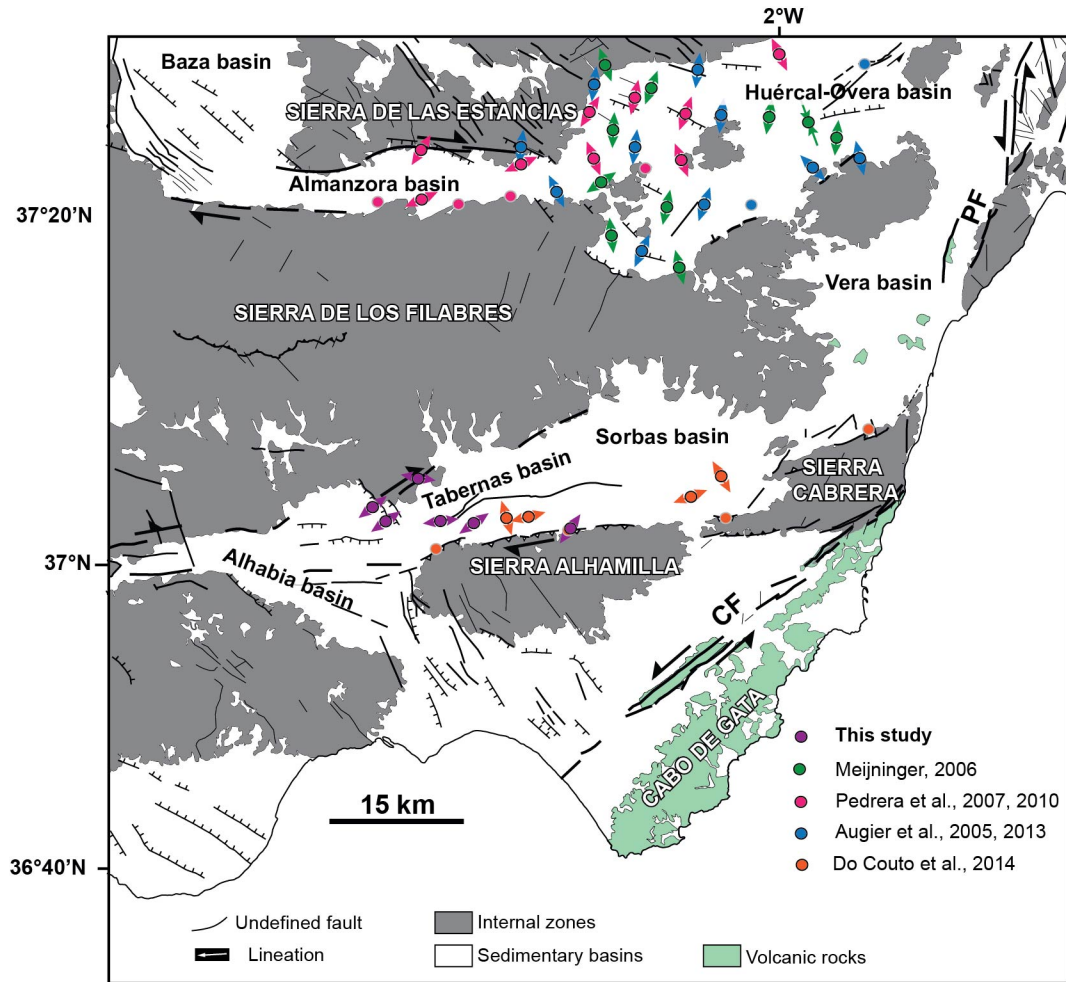
Figure 8: Synthesis of stress regimes resolved from fault slip data inversion in Tortonian basins. Color-coded circles with arrows depict tectonic sites where extension (given as arrows) is horizontal (pure extensional or strike-slip stress regimes). Sites where reverse tectonic regimes prevail are shown as circles highlighted in grey. Below, stereoplots of paleostresses σ1, σ2 and σ3 show a compilation of all brittle tectonic regimes extracted from Table S1. Collectively they define a prominent extension oriented NNE-SSW with a subordinate E-W-striking extension. CF: Carboneras Fault; PF : Palomares Fault.

4.1 EW-directed faulting: evidence for pre-Tortonian oblique extension ?

In Tortonian intramontane basins, one of the main set of faults is represented by E-W-directed faults, including ENE-WSW to ESE-WNW sets. North of the Alpujarras Corridor (AC), 3 km to the NE of Canjáyar, the contact between the basal Tortonian conglomerates and the series of Alpujarride complex is exposed in the Rambla de Tices. It is

338 shaped by a 2-meter thick fault zone (**Figs. 9a,b**) striking N100°E, which has a normal sense of slip with a right-lateral

339 strike-slip component (**Fig. 9c**). It consists of cataclastic breccias and sheared blocks (boudins) of the host rocks (**Fig.**

340 **9d**). This major fault is found along the 65 km-long Alpujarras fault zone described by Martínez-Martínez (2006) as

341 a major strike-slip dextral transfer zone south of the Sierra Nevada that acommodates both WSW-extension and dextral

342 movement. It is mechanically consistent with NE-SW/ENE-WSW extension under a strike-slip regime as resolved

343 nearby along the same faults system (Martínez-Martínez, 2006). **Fig. 9** indicates the fault is parallel to the basal

344 Tortonian series but cuts across the Alpujarride complex. In the HOB, on the southern flank of the Sierra Limaria

345 (**Fig. 8**), the unconformity between the lower Tortonian red conglomerates and the Alpujarride units (Rambla de

346 Cordoba, 2km NW Arboleas, **Figs. S1a, b**) is found reactivated as a normal fault with a dextral shear component.

347 To the North of TB, a large morphological surface presents a rare exposure of the micaschist basement of the Nevado-

348 Filabrides complex allowing the study of deformation on the southern flank of the Sierra de los Filabres (**Fig. 10**). The

349 deformed NF series shapes a kilometric-size antiform with axial planar surface dipping towards the North. The steeply-

350 dipping cleavages directed NE-SW on its southern flank are deformed by numerous dextral shear zones with lengths

351 ranging from 100 m to less than 5 m (**Fig. 10b, c**). In addition to isoclinal folds parallel to the main foliation that are

352 clearly associated to an early stage of ductile EW-stretching, we recognize close to the strike-slip shear zones, steeply-

353 dipping metric-size open to tight folds inclined to the NE (**Fig. 10d**). To the south, Tortonian conglomerates are

354 overlying unconformably the folded NF foliation. This stratigraphic relationships and the average low dip of Tortonian

355 strata (20°SE) indicate that strike-slip deformation occurred before the deposition of Tortonian conglomerates and

356 after the tilting of the NF foliation (see cross section in **Fig. 10a**). This argues that the transition from W-directed

357 ductile extension in the metamorphic domes known to have started in the Burdigalian and the right-lateral strike-slip

358 faulting occurred around the Langhian-Serravallian (13-14 Ma). This interval is often considered to mark the transition

359 from ductile to brittle extension (e.g. Augier et al., 2013). Because strike-slip faulting postdates folding of the NF

360 foliation, and are consistent with WSW-ENE oblique extension, we suggest that the Sierra de los Filabres metamorphic

361 dome formed in a transtensional strain regime. This hypothesis conforms with prediction of transtension at the tip of

362 the STEP fault (Le Pourhiet et al., 2012) and with model of oblique extension (see **Fig. 3**).

363

364
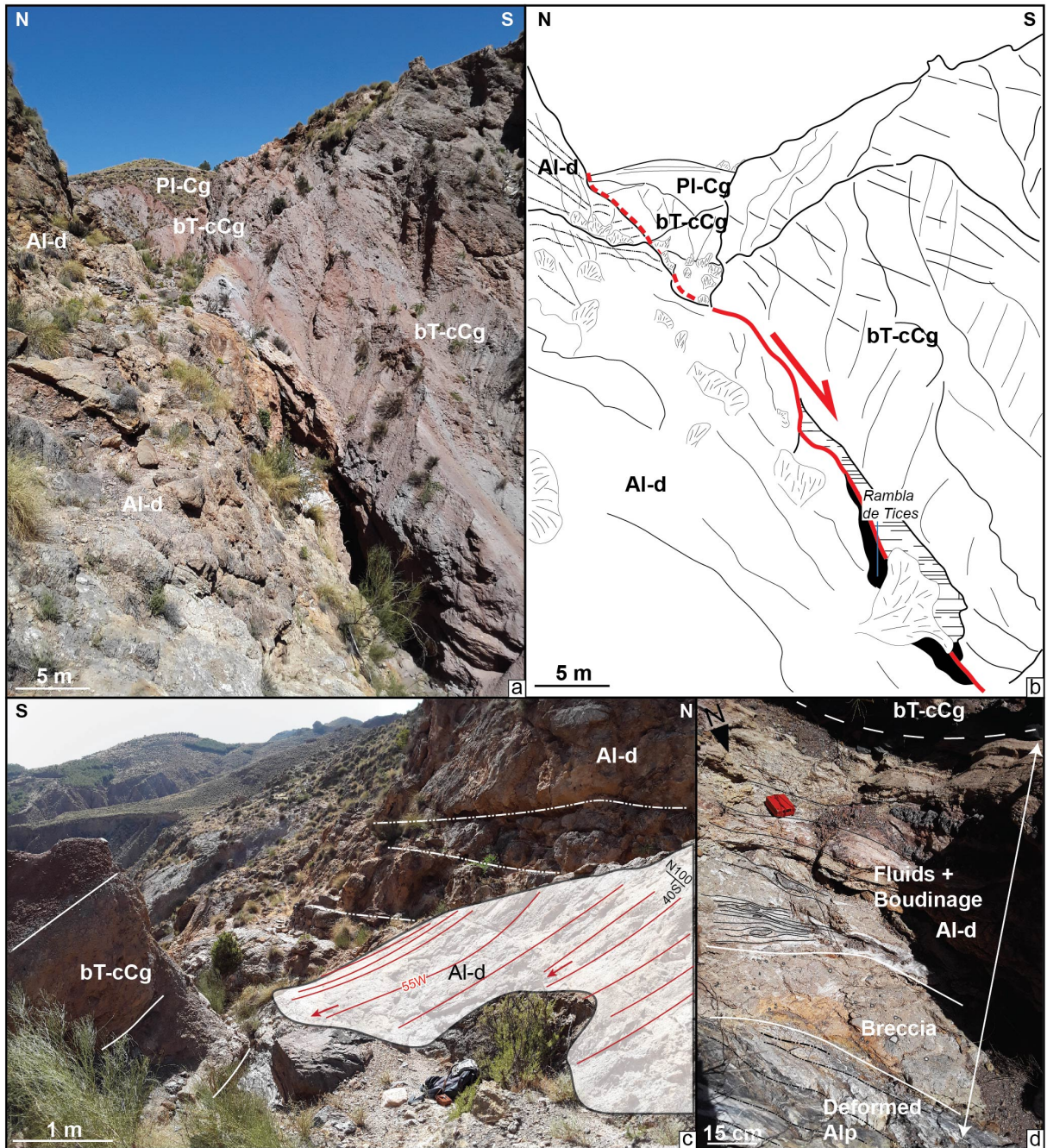
Figure 9. (a) and (b) Fault zone at the contact between the Tortonian basal conglomerates and the series of the Alpujarride complex south of AC (Rambla de Tices, see **Fig. 5** for location). (c) slikenslides on the fault zone reveasl a normal sense of slip with right-lateral strike-slip component found in association with (d) cataclastic breccias, sheared boudins of metamorphic and sedimentary rocks. Al-d: Alpujarride dolomites; bT-cCg: basal Tortonian continental Conglomerates; Pl-Cg: Pliocene Conglomerates. Coordinates 37.031944°N/-2.716274°E.

4.1.2. NW-SE-directed normal faulting

A second set is represented by NW-SE directed normal faults (**Fig. 8**). They are found, for instance, bordering the the

NE part of Alhabia basin, where they cut across the basement and interrupt the westward continuity of the southern

374 flank of the Sierra de los Filabres. One major fault zone of this system is well exposed in the Arroyo del Verdelecho,

375 7 km to the west of Tabernas, on the eastern border of the Alhabia basin (**Figs. 11 and S2**). From a regional point of

376 view this large NW-SE fault zone controls the deepening of the Tortonian basin and the position of Pliocene

377 depocenter in its hangingwall, towards the West. NW-SE normal faults also cut across the lower Tortonian

378 conglomerates in the hanginwall but their throw diminishes upward in the upper Tortonian margin sediments,

379 suggesting fault activity during the late Tortonian (**Fig. 11**). One major fault zone is outlined by cataclastic breccias

380 made of marbles originated from the exhumed Alpujarride complex in the Sierra de los Filabres (**Fig. S2**).

381 South of HOB (south of Arboleas), NW-SE faults are seen cutting through the late Tortonian sands and marls series,

382 indicating that NE-SW extension is at least Tortonian (**Figs. S1c, d**).

383
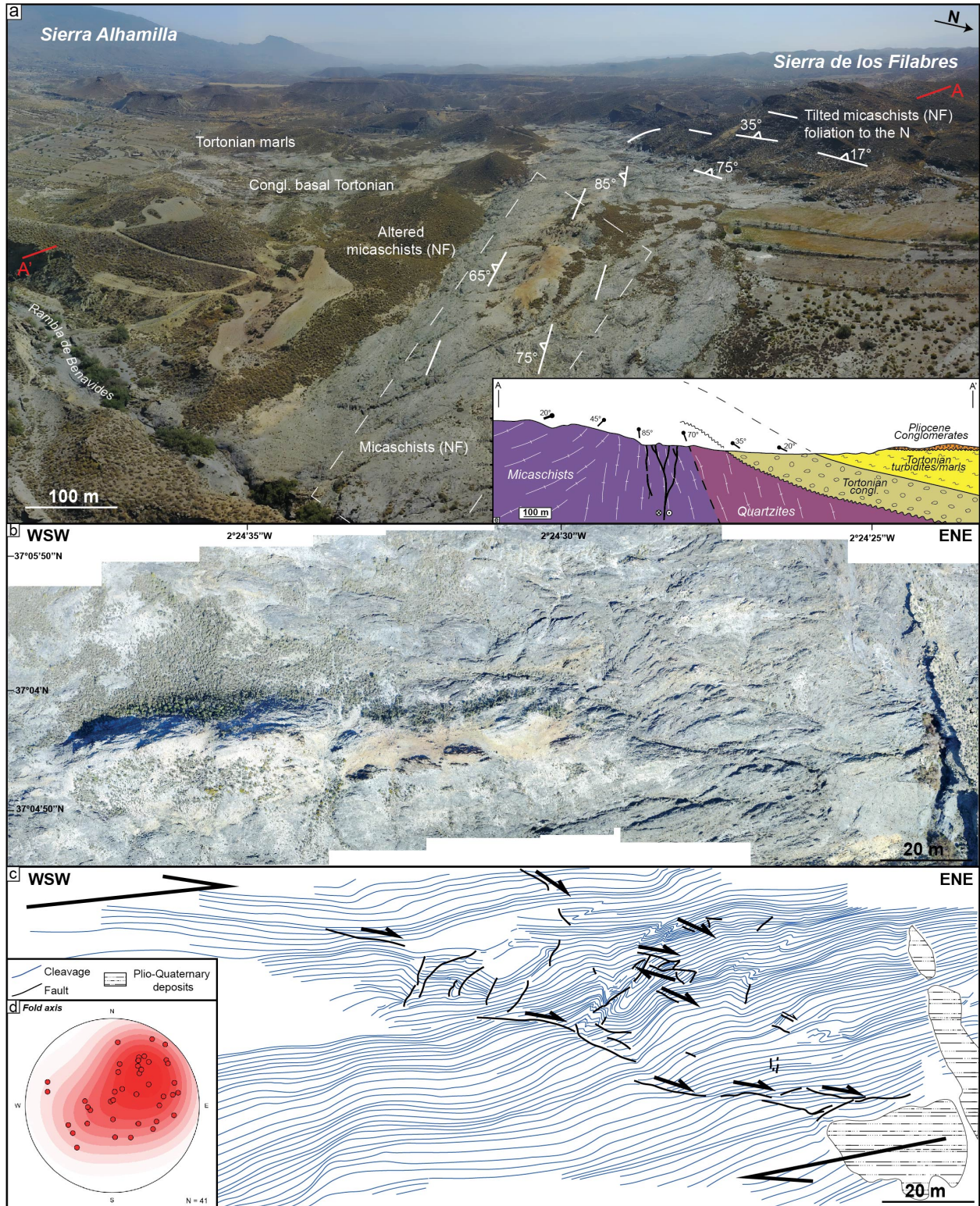
384
385 **Figure 10** : (**a**) Drone view taken in the SSW direction of the southern flank of the Sierra de los Filabres at the contact
386 with the Tabernas basin (see Figure 5 for location). Local folding of the micaschist is apparent in the right where the
387 foliation is striking NNE-SSW and is dipping ~25°E whereas it is vertical and striking SW-NE in the center of the
388 studied area forming paleosurface. Local cross section highlights the unconformable contact between the Tortonian
389 conglomerates and overlying on the basement. (**b**) High-resolution drone images of the paleosurface and (**c**) line-

390   drawing of the foliation revealing secondary folding (see (**d**) stereoplot of fold axes inclined to the NE) and dextral
391   shear zones. Coordinates 37.082777°N/-2.410544°E.
392

393

394
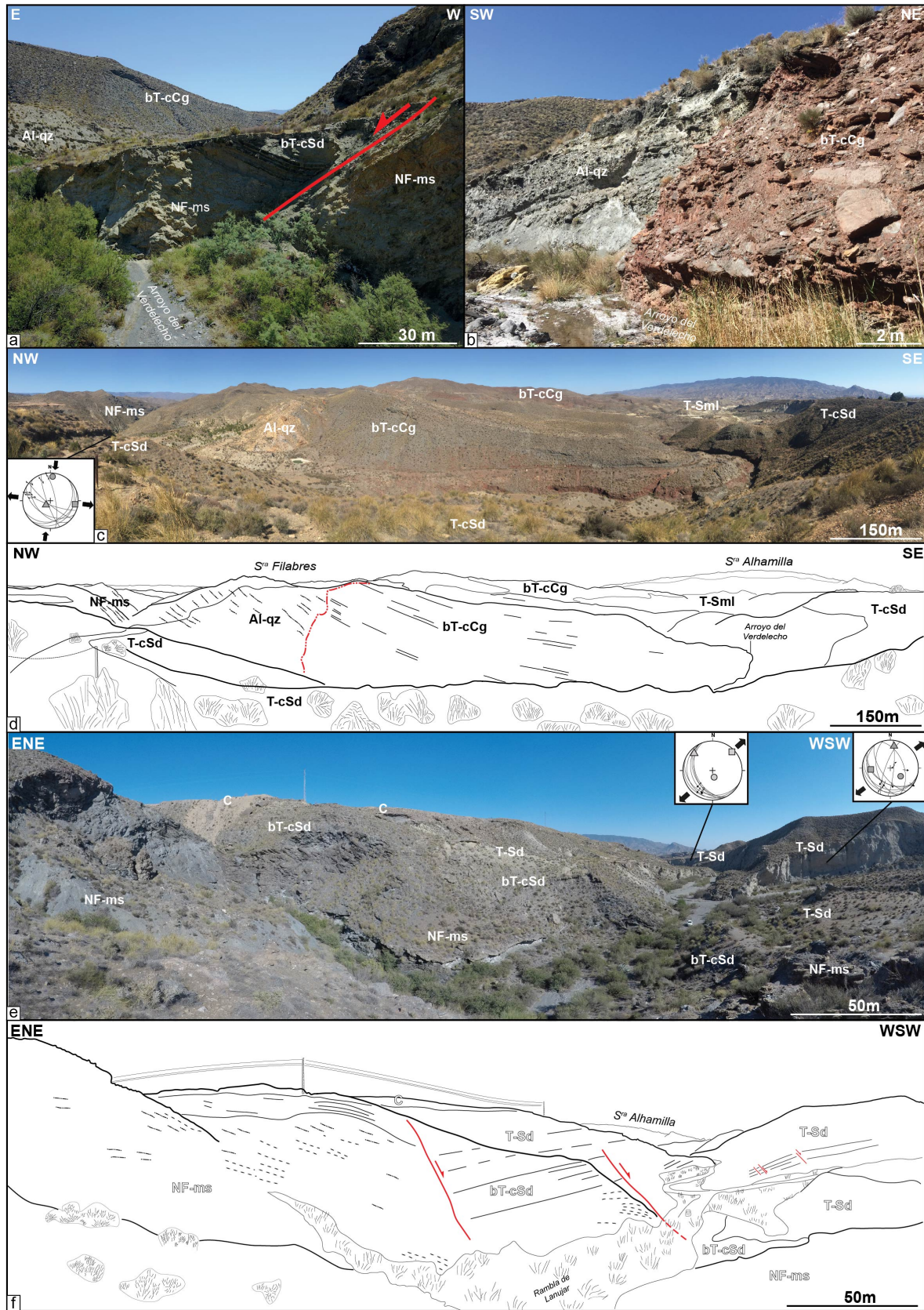
396 **Figure 11** : (**a**) Field photographs of a NW-SE normal fault at the contact between the Nevado-Filabride micaschists
397 (footwall) and Tortonian sediments (hanginwall). (**b**) Stratigraphic contact between grey and red basal Tortonian
398 continental conglomerates. These thick Tortonian series rest conformably on the Alpjuarride complex (**c**, **d**).
399 Coordinates 37.059507°N/-2.478386°E. (**e, f**) NW-SE normal faults cutting across the NF micaschists basement.
400 These faults that also affetc the early Tortonian deposits are sealed by late Tortonian deposits and are therefore syn-
401 depositional. See Figure 5 for location. Al-qz: Alpujarride quartzites; NF-ms: Nevado-Filabride micaschists; bT-cCg:
402 basal Tortonian continental Conglomerates; bT-cSd: basal Tortonian continental Sandstones; T-cSd: Tortonian coarse
403 Sandstones; T-Sd: Tortonian Sandstones; T-Sml: Tortonian Sandstones-marls; C: calcretes. Coordinates
404 37.061279°N/-2.490309°E. Paleostress orientations are in Table S1.
405

406 Both fault slip data and our own observations argue for a regional pre-Tortonian and syn-early Tortonian NNE-SSW

407 directed extension. This direction of extension is also found associated with less well-developed strike-slip regimes

408 (**Fig. 8**). It is consistent with the D1-D2 phase of brittle deformation found in HOB (Augier et al., 2013). The fact that

409 extension and strike-slip regimes occurred synchronously, or overlap rapidly in time, supports the view that they

410 reflect the same large-scale tectonic setting. The reason why strike-slip faulting is less apparent in the field than

411 expected in models in **Fig. 3** is likely to reflect the fact that oblique extension is not fully partitioned between normal

412 and strike-slip components and is actually distributed along oblique structures. Moreover, where strike-slip faults are

413 found they are associated with narrow basins or near the contact betwen the cover and basement but not in the center

414 of HOB or TB. The NNE-SSW to NW-SE faults appear to postdate the deposition of the early Tortonian red

415 conglomerates and is synchronous with the deposition of marine Tortonian series (**Fig. 12**). These normal faults

416 currently form half-graben filled with Plio-Quaternary deposits (Guadix, Baza, Alhabia) and are active today. But the

417 importance of extension-related brittle deformation over brittle compression decreases eastwards. Indeed, a late brittle

418 compressional event oriented roughly N-S is described in the literature as a D3 brittle event (e.g. in HOB) associated

419 with reverse and strike-slip faults (Augier et al., 2013). The post-late Tortonian shortening is seen responsible for fold

420 amplification and reverse faulting on the northern limb of Sierra de Alhamilla and Sierra de los Filabres, and locally

421 in the eastern part of the HOB near the termination of left-lateral strike-slip faulting evolution of the Alhama de Murcia

422 fault (**Fig. 8**).
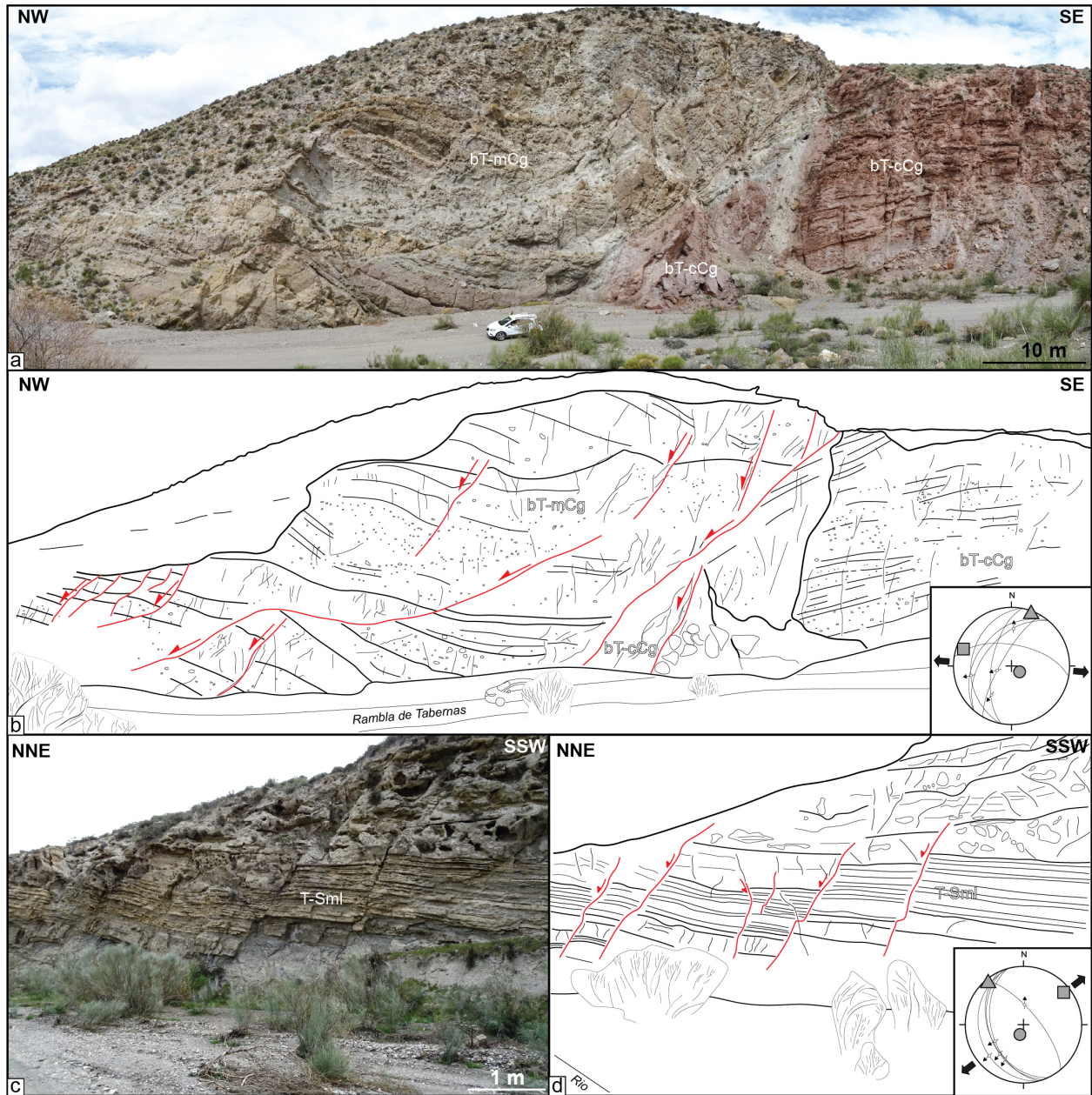
Figure 12: (**a, b**) N-S to NNE-SSW-oriented normal to dextral faults affecting the basal Tortonian continental conglomerates (bT-cCg) and marine conglomerates (bT-mCg) (Rambla de Tabernas). They form a long and tight E-W anticlinal crosses the Tabernas basin (see Figure 5 for location). (**c, d**) Several normal faults observed in Tortonian sandstones and marls (T-Sml). They are mostly oriented NNW-SSE. Coordinates 37.041648°N/-2.399318°E. Paleostress orientations are in Table S1.

5. N-S crustal-scale section across the oblique/transform margin of Alboran basin

To examine further the structural relationships between extension and strike-slip faulting across the Alboran margin, we explore 2D multichannel seismic lines acquired during the MARSIBAL 1-06 cruise (Comas and MARSIBAL1-06 Scientific Party, 2007) and ESCI cruises (Comas et al., 1995) across the Eastern Alboran basin (EAB). The studied seismic dataset consists of ~300 km and are deep-penetration multichannel seismic reflection studies (12 s two-way travel time - TWTT). Here, we study two lines namely MSB08 and MSB07 (see location in **Fig. 1**). For stratigraphic

and structural correlations between the studied seismic lines, we used the Andalucia-A1 well (**Fig. 6a**) and results from ODP 977 and 978 legs (see location in **Fig. 1**). MSB08 is striking N70°E, slightly oblique to the shoreline. It is close, and runs parallel, to TM08 line of Gómez de la Peña et al. (2018). It is calibrated by Andalucia-A1 well and ESCI-Alb1 line (Comas et al., 1995). Line MSB07 stretches in the N-S direction between the EAB in Spain and SAB to the north of Morocco parallel to line TM09 (Gómez de la Peña et al., 2018) and crosscuts line ESCI Alb2b presented in Comas et al. (1995) and Booth-Rea et al. (2007) (**Fig. 1**).

5.1 Offshore structures and stratigraphic architecture

The Carboneras Fault is well imaged north of MSB07 (**Fig. 13**). It forms a positive crustal-scale antiformal flower structure related to left-lateral strike-slip faulting that involves a Moho depth variation between 12 s to 9-8 s TWT after Gómez de la Peña et al. (2018). It separates a thin continental crust to the North (25-20 km; **Fig. 2**), from the magmatic calc-alkaline arc crust of the EAB with a thickness of 18 km in the south (Booth-Rea et al., 2007, 2018; Gómez de la Peña et al., 2018, 2020a).
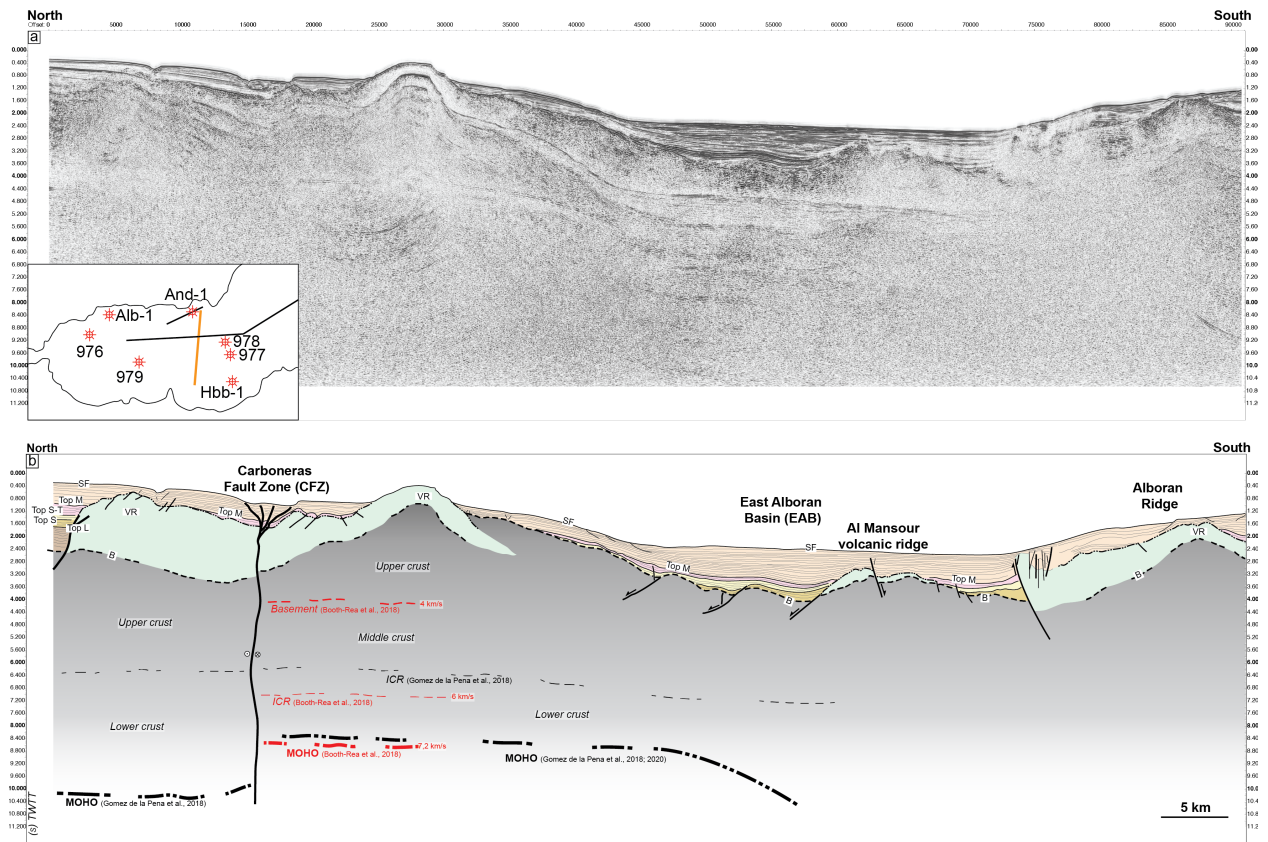
Figure 13 : Seismic reflection line MSB07 (location on **Fig. 1**). Discontinuous intracrustal reflectors (ICR) imaged between 3 and 6.5 s TWT, have been interpreted as mylonitic zones within the metamorphic basement (Carbonell et al., 1998; García-Dueñas et al., 1994; Gómez de la Peña et al., 2018). VR: Volcanic Ridge; B: Acoustic basement; Top L : Top Langian; Top S: Top Serravallian; Top S-T: top Serravallian-Tortonian; Top M: Top Messinian; SF: Seafloor.

456

457

Reflection seismic data (**Figs. 13, 14, 15**) collectively show a stratified crust, corresponding to the sediment cover, down to 2.4-4 s TWT, which outlines the acoustic basement with high reflectivity (B). Locally, the top basement reflector coincides with erosional palaeo-relief or high angle normal faults bounding basement highs. These faults are oriented mostly NW-SE to NE-SW and cut across the basement. We recognized on seismic images magmatic additions in the continental crust that are shaped by volcanic edifices exposed on the seafloor (e.g. Chella Bank) or slightly buried (Alboran Ridge) outlined by symmetric downlaps and onlaps of sediments. These constructions form topographic highs such as the Chella Bank on the MSB08 line (**Fig. 14**), the Alboran Ridge on the MSB07 line (**Fig. 13**) and the Maimonides Ridge on the ESCI-Alb2b line (**Fig. 15**). All the reflectors corresponding to layers as old as Tortonian are onlapping against the volcanic ridges confirming that the volcanic activity occurred during the middle to late Miocene times, which is shown by Duggen et al. (2008). Some reflectors up to the top Messinian (top M) onlap onto the volcanic ridges probably as a result of Pliocene uplift.

The stratigraphy offshore, on the continental crustal domain, is defined by the recognition of five seismic stratigraphic units in Andalucía-A1 well (Jurado and Comas, 1992) labeled I-V from top to base (**Figs 6** and **16**) and separated by unconformities. The seismostratigraphic units I to V vary in thickness **(Fig. 16)** and their architecture is conditioned by the occurrence of basement highs and crustal-scale faults.

Below the Miocene sedimentary filling, Andalucia-A1 well reveals ~190m of phyllitic and quartzitic meta-sediments (2.4 to 4 s TWT below the Alboran basin, **Figs. 13** and **14**) topped by Langhian to Tortonian marls (top at ~1.6 to 3.4 s TWT below the Alboran basin) interbedded with Tortonian-Messinian tuffs and basaltic lavas. These units have been correlated in the magmatic arc crust of EAB after Gómez de la Peña et al. (2020b). The older deposits (Unit V) Langhian-Serravallian in age, consist of clays and marls with intercalated sands and volcano-clastic deposits. The seismic facies of this Unit V is made of moderate amplitude and low frequency discontinuous reflections packages (Figure 18), and is only present in the Northern Alboran Basin. They are correlated with volcanic series in the EAB (vY3) (Gómez de la Peña et al., 2020b). They pass upward into Serravallian sand-silty clay turbidite (Unit IV) possibly correlated with volcanic series in EAB (vY2 after Gómez de la Peña et al., 2020b). This unit exhibiting low to moderate amplitude, moderate frequency drawing continuous sheeted to disrupted reflectors, is unconformably overlying Unit V and locally onlaps onto the basement. Thickness of Unit IV remains rather thin in the North and East Alboran Basin. It can't be properly identified in the South Balearic Basin, east of the Maimonides volcanic ridge (**Fig. 15**). The Unit III dated from late Serravallian to late Tortonian is represented by sandstones interbedded with volcano-clastic levels whih correlates in EAB with volanics vY1 unit. Unit III contains internal reflections characterized by low to moderate amplitude, moderate frequency continuous sheeted reflectors. Its thickness remains relatively constant from the NAB to the EAB, and is identified beneath the Messinian Unit II in the South Balearic Basin. Unit II corresponds to the Messinian evaporite, carbonate, volcanic, and volcaniclastic deposits interbedded with fine-grained sediments and is equivalent to unit III of Gómez de la Peña et al. (2020b) in EAB. Seismic facies of Unit II is marked in the Alboran domain by lower amplitudes and lower frequency reflectors. In ESCI-Alb2b line, Unit II increases drastically east of the Maimonides ridge, which delimits the western boundary of the salt deposits in the Western Mediterranean basin

during the Messinian Salinity Crisis (Haq et al., 2020). Unit II is topped by Unit I made of Pliocene to Quaternary clays and sanstones, which are correlated with units II and I in EAB (Gómez de la Peña et al., 2020b). Unit I is marked by thinly bedded, mostly parallel, high-frequency and low amplitudes reflectors (**Fig. 15**). Its thickness fluctuates in response to sedimentary processes (Juan et al., 2016).

Along line MSB08 (**Fig. 14**) the Langhian-Serravallian (Unit V) is maximum 1600 m-thick (using a P-wave velocity of 3.2 km/s calculated within Andalucia-A1 well). In EAB, south of Carboneras Fault Zone, the total thickness of Unit V is only ~300 m on MSB07 (**Fig. 13**) and is absent in ESCI-Alb2b (**Fig. 15**). The Serravallian-Tortonian (Unit IV-III) interval shows only very limited sediment accumulation (~300 m) except near the NW-SE oriented normal faults where growth geometries are visible. These normal faults are sealed by the Tortonian-Messinian deposits, indicating a syn-sedimentary faulting during the middle Miocene (**Fig. 13**). With respect to onshore observations this sedimentary infill is more continuous and is also much thinner compared to TB and HOB where they are represented by thick conglomerates and marls/turbidites (> 1km) (**Fig. 7**), and they are eroded or not deposited along the axes of the metamorphic domes. The Messinian deposits (Unit II) are ~150-350 m-thick north of CF (MSB07-08 ; **Figs. 13, 14**) and increase to about 1200 m eastward in the eastern EAB (ESCI-Alb2b ; **Fig. 15**), and in Algero-Balearic basin (Gómez de la Peña et al., 2020b). The top Messinian reflector is topped by thick horizontal sedimentary strata, with a maximum thickness of 1.2 s TWT (~2.4 km assuming a velocity of 2 km/s) on line MSB07, suggesting an important channel system during the Pliocene.

The Pliocene-to-Quaternary series are poorly deformed except in the vicinity of CF and near the Alboran Ridge where this is associated with south-dipping reverse fault (**Fig. 13**). This late and still active compressional tectonics is revealed by the overthrusting of the SAB over the south margin of the EAB (e.g. Martínez-García et al., 2011).
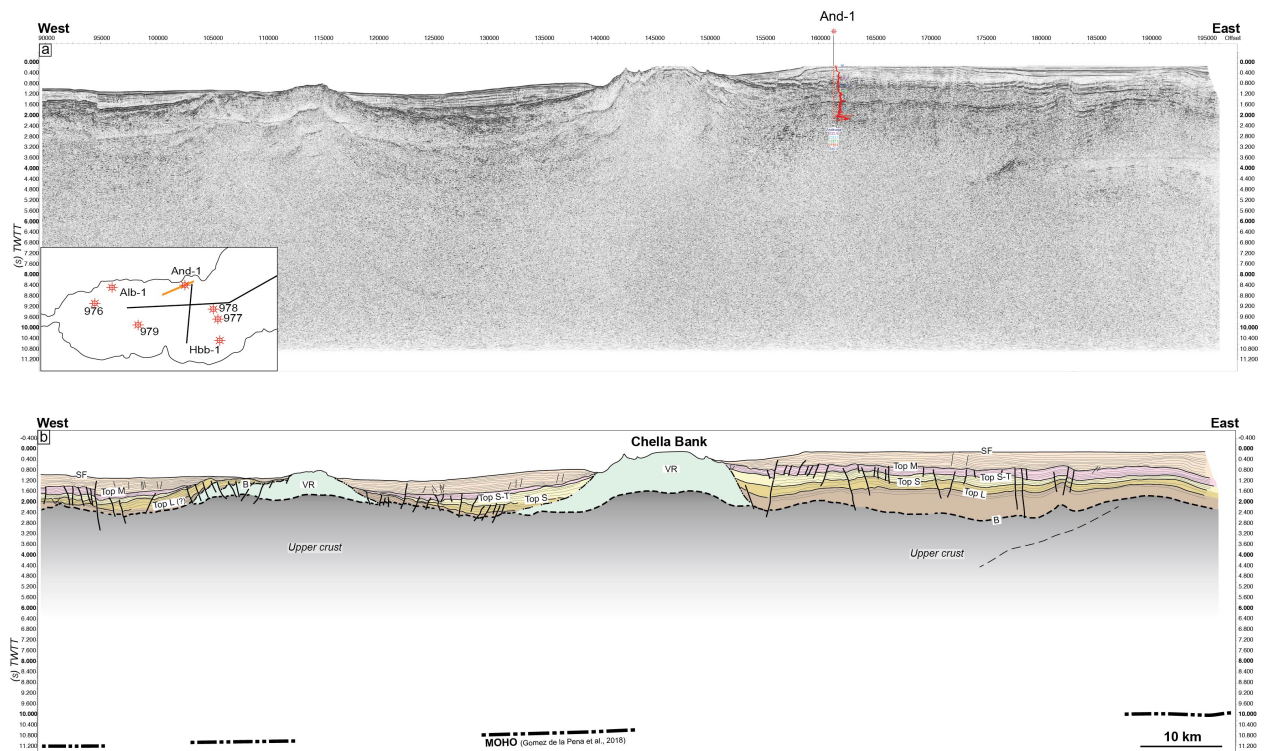
 Figure 14 : Seismic reflection line MSB08 (see location on **Fig. 1**). See Figure 13 for abbreviations. See also Figure
S3 showing a zoom on the main seismic facies recognized in Andalucia-A1 well.
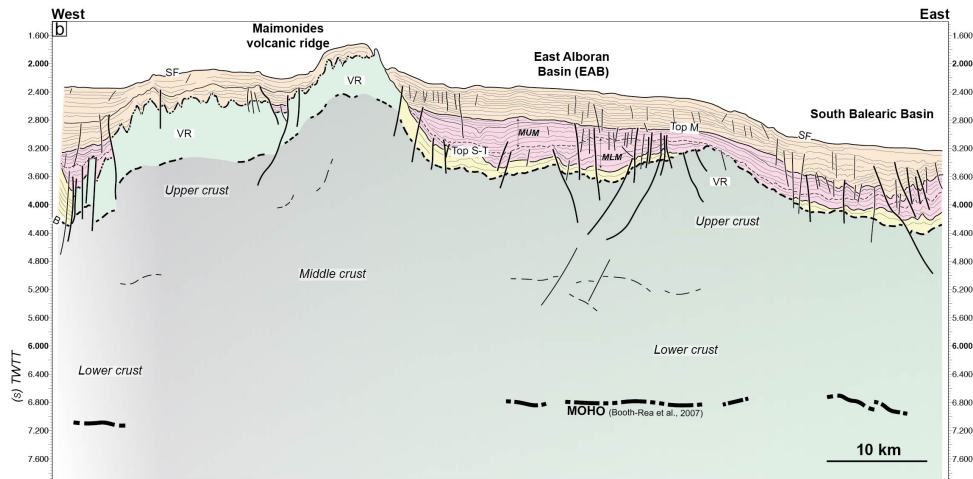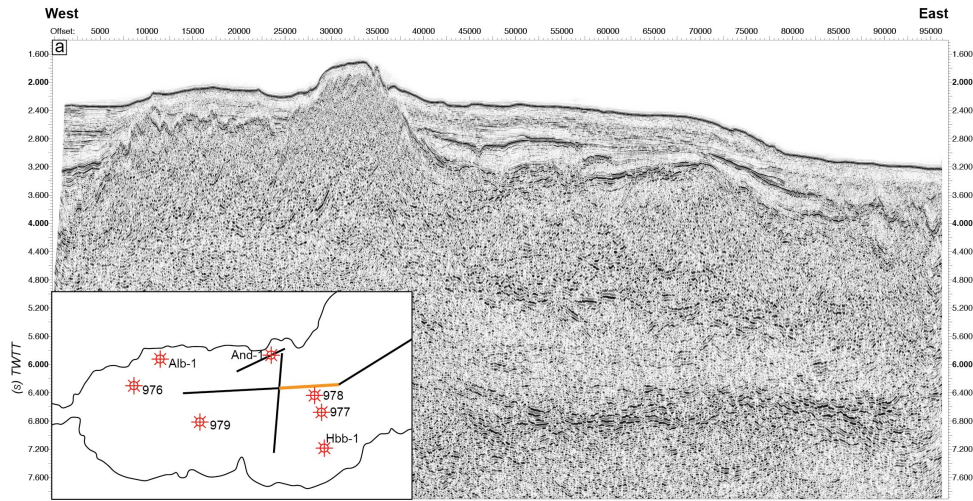
Figure 15. (**a, b**) Seismic reflection line ESCI-Alb2b and intepretation (see Figure 1 for location). Seismic units are
correlated with those defined by Booth-Rea et al. (2007). See Figure 13 for abbreviations.
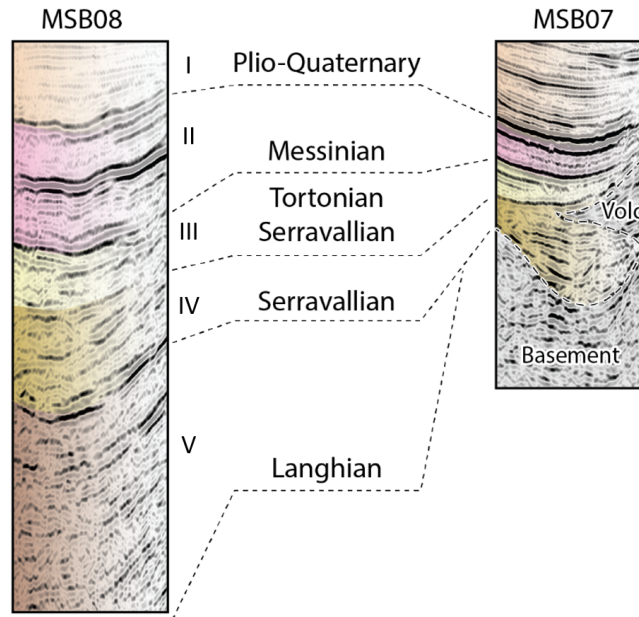
523

524 **Figure 16** : Seismic facies of units I to V seen through seismic lines MSB08 close to the shoreline and the line
525 MSB07, located deeper in the East Alboran Basin.

526 **5.2 N-S crustal cross-section of the Alboran margin accounting for strike-slip faulting**

527 Based on subsurface constraints and field data, we present in Figure 17 a crustal-scale section across the rifted margin,

528 from the Sierra de las Estancias and Huercal-Overa basin (HOB) to the Alboran ridge that represents the inverted

529 southern margin of the EAB (**Fig. 17**). The proximal margin, where the crust is 30-35 km-thick, is defined to the North

530 by the transition between the south Iberia margin, and the metamorphic domain of the Alboran basement exposed in

531 the Sierra de las Estancias. This continental domain preserves part of the crustal thickness acquired during former

532 Betic orogenic phase that has been little involved in crustal thinning. The onset of crustal thinning to the south

533 coincides with the position of the lithospheric tear fault documented by seismology (**Fig. 4**; Mancilla et al., 2015a)

534 and is recorded by the formation of asymmetric basins of the HOB and TB, shaping the upper neck domain. Orthogonal

535 and oblique extension in this domain is accommodated by normal and strike-slip faulting during the Tortonian. From

536 the Sierra de los Filabres to the south, the thickness of the continental crust reduces to 25 km in the Tabernas basin

537 along the Alpujarras strike-slip fault zone and below the Sierra Alhamilla (**Fig. 17**). The Nijar basin depicts the

538 transition towards offshore distal domains where the continental crust reaches a thickness of 20 km. The Tortonian

539 and Messinian marine sediments are also thicker. It is worth noting that a number of volcanic bodies offshore (e.g.

540 Chella Bank on MSB08) accompany crustal thinning of the continental crust. The Carboneras Fault (CF) brings crusts

541 with different thicknesses and composition into contact. South of CF, the crustal thickness of the EAB is 18 km and

542 seismic velocities, especially the occurrence of a high-Vp lower crust, has been considered to indicate the EAB is

543 floored by a magmatic arc crust (Gómez de la Peña et al., 2018; 2020), formed in a supra-subduction context above

544 the subducting Alboran slab (Booth-Rea et al., 2018). The crustal thickness of the EAB is compatible with crustal

545 thinning of the continental margin, and the occurrence of NW-SE-trending faults also recognized onshore despite

546 being slightly older (Serravalian-Tortonian) suggest that the EAB formed under the same back-arc extension setting,

547 relative to westward slab retreat as the whole Alboran margin did. Thus, the magmatic arc crust of the EAB could
548 represent voluminous magmatic intrusions (e.g. Al Mansour dacite, Alboran Ridge rhyolite dated to ca. 9 Ma; Duggen
549 et al., 2004; **Fig 17**) formed on the distal rifted margin of Alboran. The investigation of the causes of calc-alkaline
550 magmatism is beyond the scope of this study, but we suspect it reflects post-subduction arc magmatism induced by
551 remelting, during extension or delamination, of a metasomatized wedge of mantle lithosphere formed during a
552 previous subduction event (e.g. Richards, 2009). Crustal shortening in **Figure 17** is be distributed across the CF and
553 EBSZ strike-slip fault zones, north-vergent reverse faults below the Alboran Ridge and on the northern limb of Sierra
554 de Alhamilla.
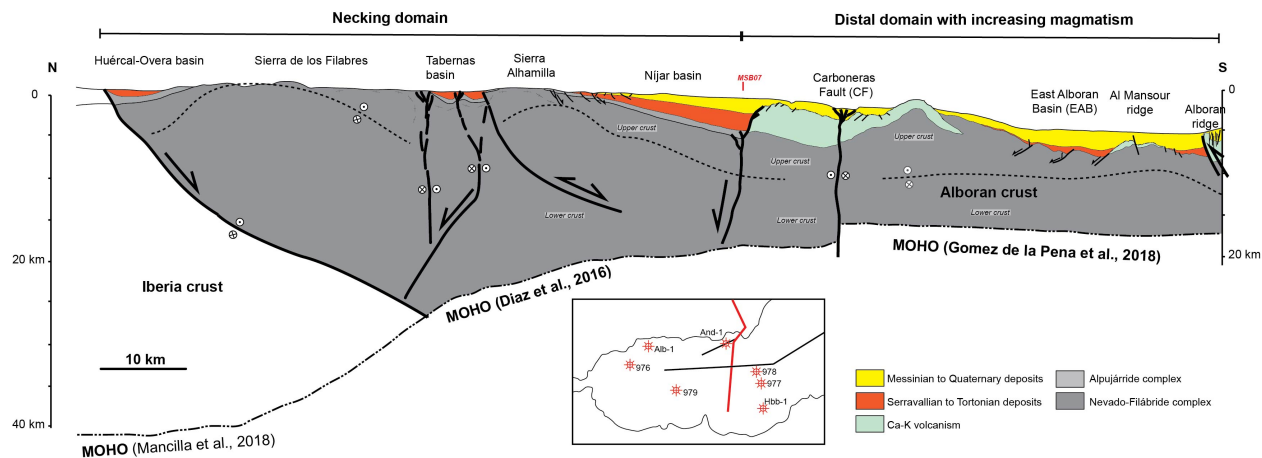
555

556 **Figure 17**. Crustal-scale cross section of the Alboran margin in the eastern Betics interpreted based on onshore and
557 offshore contraints presented in the text. Note that in the necking domain the extension of faults downwards to
558 Moho depths is not imaged on the seismics and therefore largely inspired by inferences from 3D numerical models
559 (see Fig. 3).

560
561

6. Implications

The question of whether the Miocene tectonic evolution of the Betics reflects crustal thinning associated with oblique back-arc rifting as suggested from present-day strain patterns is unclear in the literature. We found based on a comparison between numerical models and basin analyses, fault kinematics and structure of the margin in the eastern Betics compelling evidences that crustal thinning was controlled by oblique extension. Oblique rifting operated since at least the middle Miocene in relation with Alboran slab retreat below the Alboran basin and is kinematically associated with slab tearing and delamination below the central and eastern Betics.

One of the most striking tectonic feature of the Alboran margin (**Fig. 17**) is the abrupt N-S crustal thinning oblique to the direction of slab rollback. The history of sediment infill and rates of subsidence in intramontane basins (**Figs. 6 and 7**) combined with the analyses of fault slip data, and structural data offshore, confirm that brittle extension oriented from N20°E to EW occurred during an interval spanning from the Serravallian-early Tortonian to the late Tortonian (14-8 Ma) (**Fig. 18**). This extension is found associated with both normal and strike-slip regimes. Field tectonic data reveal that N20°E extension is more represented in HOB while the ENE-WSW to EW extension is found related with the evolution of the Almanzora fault zone, Alpujarras fault zone and Tabernas basin flanking the metamorphic domes (**Table S1**). There are additional evidence that EW-directed dextral strike-slip faulting occurred during the Tortonian to the South and West of the HOB. These large-scale transfer fault zones positioned on the slab edge accommodate the differential westward extension that are later cut by Tortonian NW-SE faults. These second set of faults is also observed in the magmatic crust of the EAB offshore but seismic data indicate they are Serravallian-Tortonian in age and therefore older than those identified onshore. We suggest that NW-SE normal faulting could have initiated in the EAB then migrated towards the necking domain, which was dominated by transfer faulting, as slab retreat progressed and the region affected crustal thinning widened (**Fig. 18**). Subsidence during the Serravallian-Tortonian was also lower in the magmatic crust of the EAB compared to intramontane basins onshore. This suggest that the isostatic effect of crustal thinning was compensated by a thermal anomaly in the mantle, heralding the Ca-K magmatism at 11-7 Ma (Duggen et al., 2004, 2008).

587
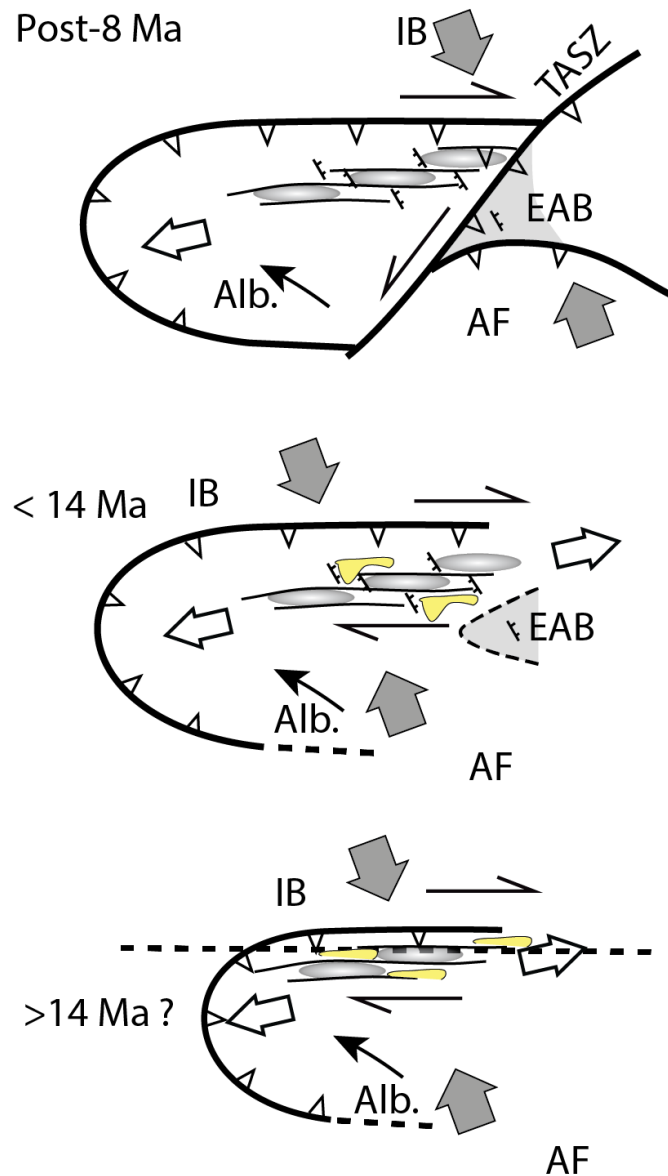
Figure 18: Tectonic model of the evolution of the northern margin of the Alboran Rift. Large grey and white double arrows depict shortening, which is parallel to the AF/IB convergence, and the highly oblique extension, respectively. The thin black arrows show the motion of Alboran relative to Iberia (IB) taken from Figure 4. Half arrows depict distributed strike-slip faulting in the Betics. NW-SE directed normal fault and strike-slip basins (yellow) are consistent with the oblique extension. Grey-shaded ellipses represent the metamorphic domes. TASZ : simplified representation of the Trans-Alboran Shear Zone. We also indicated EAB which mostly formed ca. 9 Ma (Duggen et al., 2004; Booth-Rea et al., 2018).

595

596   Several key tectonic features found in the eastern Betics are predicted by 3D models of oblique extension (**Figure 3**).

597   They include E-W trending normal faults that are prevalent on the upper neck domain (i.e. Sierra de las Estancias and

598   HOB), and E-W strike-slip faults (Almanzora and Alpujarras fault zones). NW-SE normal faults are associated with

599 more distal domains on the continental margin where crustal thinning is the highest offshore, south of Nijar basin, and

600 in the EAB.

601 Tectonic inversion seems, in contrast, to have been increasingly more important when approaching the Carboneras

602 and Palomares strike-slip faults in the East since the late Tortonian.

603 Ductile thinning associated with the formation of metamorphic domes and exhumation of HP rocks is dated to 23 to

604 16 Ma (Platt et al., 2006; Booth-Rea et al., 2015). This provides time constraint for the beginning of oblique extension

605 and westward slab rollback. Deformation at the future location of the tear fault was probably initially diffuse and

606 resulted in an immature oblique rift system in the South, combined with thrusting in the external zones to the North

607 (**Figure 18**). In the Langhian-Serravallian (14-13 Ma), accompanying slab steepening, localization of slab tearing, and

608 propagation of thrusting in external zones, oblique extension spread over the whole central Betics. At this time,

609 metamorphic domes exhumed to upper crustal levels and recorded the transition from ductile shearing to brittle

610 faulting (**Figure 18**). Brittle E-W-directed stretching and dextral transcurrent deformation formed at this time. The

611 late/post-Tortonian times (~8 Ma) marks a change in the tectonic evolution of the Betics and Alboran domain as the

612 mantle slab detached with no further westward slab retreat (van Hinsbergen et al., 2014; Do Couto et al., 2014;

613 Martínez-García et al., 2017; d'Acremont et al., 2020; García-Castellanos and Villaseñor, 2011; Spakman et al., 2018).

614 This regional event is synchronous with the cessation of extension and onset of uplift in the western Mediterranean

615 region and Iberia (Jolivet et al., 2021a; Mouthereau et al., 2021; Rat et al., 2022). Ca-K magmatism occurred between

616 11 and 7 Ma and was followed, east of EBSZ, by the indendation by the magmatic crust of the EAB in the Águilas

617 Arc (Ercilla et al., 2022), and amplification of the metamorphic domes in the vicinity of the EBSZ (e.g. Alhamilla)

618 (**Figure 18**).

619 In this model, ductile stretching and ductile detachment associated with the development of the domes are the

620 expression of oblique E-W extension. It provides a coherent scheme linking the formation of EW-directed basins in

621 the brittle field associated with strike-slip faulting, and NW-SE/NNW-SSE sedimentary basins (Guadix, Baza,

622 Alhabia) formed in transtension during the Tortonian. As such, the oblique extension is closely associated with STEP

623 faulting required by westward slab rollback. The oblique rifting model we propose explain the formation of the

624 metamorphic domes and intermontane basins and provides insight into crustal deformation, which is broadly

625 consistent with the geodynamic models of slab rollback and tearing since 20 Ma that have been previously proposed

626 for Alboran (Chertova et al., 2014; Spakman et al., 2018). In the latter models, however, the ENE-WSW extension in

627 the central-eastern Betics is related to differential absolute motions between Iberia and the slab decoupled from Iberia

628 by slab tearing. In our scenario, oblique extension is entirely related to westward lateral rollback. It can not be

629 excluded, however, that the effect of mantle-derived slab dragging increased during the late extensional stage, from

630 14-13 Ma, when slab tearing localized.

631 Mid-Miocene high-pressure metamorphism documented in the central Betics (Platt et al., 2013) was synchronous with

632 slab steepening and subduction that was under way during oblique back-arc extension (**Figure 18**). The case of

633 exhumation of high-pressure rocks in oblique convergence setting associated with near-parallel orogen extension is

634 also documented in other active orogen like Taiwan (Conand et al., 2020).

635   This highly oblique northern Alboran margin differs from typical transform fault margin such as those associated with
636   the Altantic ocean because it accommodates variations in intra-plate extensional movements, triggered by slab roll-
637   back, not variations in spreading rates. Strike-slip faults may have originated as low-angle normal faults which were
638   later reactivated as thrusts during margin inversion. Similar observations, including metamorphism, strike-slip
639   faulting, high geothermal gradients and volcanism has been made in Seram, north of the Banda Arc, which represents
640   another example of extremely thinned crust formed perpendicular to the direction of the slab rollback (Pownall et al.,
641   2013). Such a narrow rifted margin associated with lithospheric STEP fault defines a class of oblique margin that is
642   expected to be hardly preserved in the geological record due the transient nature of retreating subduction systems.
643
644

645   **Data availability**.This study is based on data compilation. Data used in this study can be found in the appropriate
646   references. Paleostress tensors obtained by the inversion of fault slip data are available online in the Supplement.
647

648   **Supplement**.The supplement related to this article is available on-line at:
649

650   **Competing interests**.The authors declare that they have no conflictof interest.

651   **Authors contribution**
652   ML and FM, conceptualize, prepared figures and tables, compiled and interpreted field structural data and wrote the
653   paper. DC provided and interpreted the seismic lines, reviewed the text and contributed to the writing. AJ carefully
654   exmined the implementation of his numerical results and reviewed the text. EM, SC and VM, supervised and
655   coordinate the different project tasks and reviewed the text.

656   **Acknowledgments**
657   Víctor Tendero Salmerón, Guillermo Booth-Rea, and an anonymous reviewers are warmly thanked for their comments
658   that greatly improved the manuscript. The stereogram results were obtained using Win-Tensor, a software developed
659   by Dr. Damien Delvaux, Royal Museum for Central Africa, Tervuren, Belgium (Delvaux and Sperner, 2003). The
660   processed seismic data were interpreted using Kingdom IHS Suite© software. This research benefited from
661   discussions and support of OROGEN project, an academic-industry research consortium between TOTAL, CNRS and
662   BRGM.

663
664

References

666 Angrand, P., Mouthereau, F., 2021. Evolution of the Alpine orogenic belts in the Western Mediterranean region as
667   resolved by the kinematics of the Europe-Africa diffuse plate boundary. Bsgf - Earth Sci Bulletin.
668   https://doi.org/10.1051/bsgf/2021031
669 Argus, D.F., Gordon, R.G., DeMets, C., 2011. Geologically current motion of 56 plates relative to the no-net-
670   rotation reference frame. Geochemistry, Geophysics, Geosystems 12. https://doi.org/10.1029/2011gc003751
671 Augier, R., 2004. Evolution tardi-orogénique des Cordillères Betiques (Espagne) : apports d'une étude integrée 1
672   vol., [II]-400 p.
673 Augier, R, Agard, P., Monié, P., Jolivet, L., Robin, C., Booth-Rea, G., 2005. Exhumation, doming and slab retreat in
674   the Betic Cordillera (SE Spain): in situ40Ar/39Ar ages and P–T–d–t paths for the Nevado-Filabride complex.
675   Journal of Metamorphic Geology 23, 357–381. https://doi.org/10.1111/j.1525-1314.2005.00581.x
676 Augier, R., Booth-Rea, G., Agard, P., Martínez-Martínez, J.M., Jolivet, L., Azañón, J.M., 2005a. Exhumation
677   constraints for the lower Nevado-Filabride Complex (Betic Cordillera, SE Spain): a Raman thermometry and
678   Tweequ multiequilibrium thermobarometry approach. Bulletin de la Societe Geologique de France 176, 403–
679   416. https://doi.org/10.2113/176.5.403
680 Augier, R., Jolivet, L., couto, D.D., Negro, F., 2013. From ductile to brittle, late- to post-orogenic evolution of the
681   Betic Cordillera: Structural insights from the northeastern Internal zones. Bulletin De La Société Géologique De
682   France 184, 405–425. https://doi.org/10.2113/gssgfbull.184.4-5.405
683 Augier, R., Jolivet, L., Robin, C., 2005b. Late Orogenic doming in the eastern Betic Cordilleras: Final exhumation
684   of the Nevado-Filabride complex and its relation to basin genesis. Tectonics 24, n/a-n/a.
685   https://doi.org/10.1029/2004tc001687
686 Badji, R., Charvis, P., Bracene, R., Galve, A., Badsi, M., Ribodetti, A., Benaissa, Z., Klingelhoefer, F., Medaouri,
687   M., Beslier, M.-O., 2014. Geophysical evidence for a transform margin offshore Western Algeria: a witness of a
688   subduction-transform edge propagator? Geophys J Int 200, 1029–1045. https://doi.org/10.1093/gji/ggu454
689 Baudouy, L., Haughton, P.D.W., Walsh, J.J., 2021. Evolution of a Fault-Controlled, Deep-Water Sub-Basin,
690   Tabernas, SE Spain. Frontiers Earth Sci 9, 767286. https://doi.org/10.3389/feart.2021.767286.
691 Bessière, E., Jolivet, L., Augier, R., Scaillet, S., Précigout, J., Azañon, J.-M., Crespo-Blanc, A., Masini, E., Couto,
692   D.D., 2021. Lateral variations of pressure-temperature evolution in non-cylindrical orogens and 3-D subduction
693   dynamics: the Betic-Rif Cordillera example. Bsgf - Earth Sci Bulletin. https://doi.org/10.1051/bsgf/2021007
694 Bezada, M.J., Humphreys, E.D., Toomey, D.R., Harnafi, M., Dávila, J.M., Gallart, J., 2013. Evidence for slab
695   rollback in westernmost Mediterranean from improved upper mantle imaging. Earth and Planetary Science
696   Letters 368, 51–60. https://doi.org/10.1016/j.epsl.2013.02.024
697 Booth-Rea, G., Martínez-Martínez, J.M., Giaconia, F., 2015. Continental subduction, intracrustal shortening, and
698   coeval upper-crustal extension: P-T evolution of subducted south Iberian paleomargin metapelites (Betics, SE
699   Spain). Tectonophysics 663, 122–139. https://doi.org/10.1016/j.tecto.2015.08.036
700 Booth-Rea, G., Ranero, C.R., Grevemeyer, I., 2018. The Alboran volcanic-arc modulated the Messinian faunal
701   exchange and salinity crisis. Scientific reports 8, 13015. https://doi.org/10.1038/s41598-018-31307-7
702 Booth-Rea, G., Ranero, C.R., Martinez-Martinez, J.M., Grevemeyer, I., 2007. Crustal types and Tertiary tectonic
703   evolution of the Alborán sea, western Mediterranean. Geochemistry, Geophysics, Geosystems 8, n/a-n/a.
704   https://doi.org/10.1029/2007gc001639
705 Booth-Rea, G., Azañón, J.-M., Azor, A., García-Dueñas, V., 2004. Influence of strike-slip fault segmentation on
706   drainage evolution and topography. A case study: the Palomares Fault Zone (southeastern Betics, Spain). J
707   Struct Geol 26, 1615–1632. https://doi.org/10.1016/j.jsg.2004.01.007
708 Borque, M.J., Alzola, A.S., Martin-Rojas, I., Alfaro, P., Molina, S., Cintas, S.R., Caderot, G.R., Lacy, C., Avilés,
709   M., Olmo, A.H., Tortosa, F.J.G., Estévez, A., Gil, A.J., 2019. How Much Nubia-Eurasia Convergence Is
710   Accommodated by the NE End of the Eastern Betic Shear Zone (SE Spain)? Constraints From GPS Velocities.
711   Tectonics 38, 271–1839. https://doi.org/10.1029/2018tc004970
712 Braga, J.C., Martín, J.M., Quesada, C., 2003. Patterns and average rates of late Neogene–Recent uplift of the Betic
713   Cordillera, SE Spain. Geomorphology 50, 3–26. https://doi.org/10.1016/s0169-555x(02)00205-2
714 Carbonell, R., Sallares, V., Pous, J., Dañobeitia, J.J., Queralt, P., Ledo, J.J., Dueñas, V.G., 1998. A multidisciplinary
715   geophysical study in the Betic chain (southern Iberia Peninsula). Tectonophysics 288, 137–152.
716   https://doi.org/10.1016/s0040-1951(97)00289-8
717 Clark, S.J.P., Dempster, T.J., 2009. The record of tectonic denudation and erosion in an emerging orogen: an apatite
718   fission-track study of the Sierra Nevada, southern Spain. Journal of the Geological Society 166, 87–100.
719   https://doi.org/10.1144/0016-76492008-041

Comas, M. C., J. J. Dañobeitia, J. Alvarez-Maron, and J. I. Soto (1995), Crustal reflections and structure in the Alboran Basin. Preliminary results of the ESCI-Alboran survey, Rev. Soc. Geol. Esp., 8(4), 529 – 542.

Comas, M.C., García-Dueñas, V., Jurado, M.J., 1992. Neogene tectonic evolution of the Alboran Sea from MCS data. Geo-mar Lett 12, 157–164. https://doi.org/10.1007/bf02084927

Comas, M., and MARSIBAL 1-06 Scientific Party (2007). Preliminary results of Marsibal 1-06 cruise in the Alboran and western Algero-Balearic basins. Geophys. Res. Abst., 9, 10871.

Conand, C., Mouthereau, F., Ganne, J., Lin, A.T., Lahfid, A., Daudet, M., Mesalles, L., Giletycz, S., Bonzani, M., 2020. Strain Partitioning and Exhumation in Oblique Taiwan Collision: Role of Rift Architecture and Plate Kinematics. Tectonics 39, e2019TC005798. https://doi.org/10.1029/2019tc005798

Crespo-Blanc, A., Comas, M., Balanyá, J.C., 2016. Clues for a Tortonian reconstruction of the Gibraltar Arc: Structural pattern, deformation diachronism and block rotations. Tectonophysics 683, 308–324. https://doi.org/10.1016/j.tecto.2016.05.045

d'Acremont, E., Lafosse, M., Rabaute, A., Teurquety, G., Couto, D.D., Ercilla, G., Juan, C., Lépinay, B.M., Lafuerza, S., Galindo-Zaldivar, J., Estrada, F., Vazquez, J.T., Leroy, S., Poort, J., Ammar, A., Gorini, C., 2020. Polyphase Tectonic Evolution of Fore-Arc Basin Related to STEP Fault as Revealed by Seismic Reflection Data From the Alboran Sea (W-Mediterranean). Tectonics 39. https://doi.org/10.1029/2019tc005885

Dalziel, I.W.D., Lawver, L.A., Norton, I.O., Gahagan, L.M., 2013. The Scotia Arc: Genesis, Evolution, Global Significance. Annu Rev Earth Pl Sc 41, 767–793. https://doi.org/10.1146/annurev-earth-050212-124155

Daudet, M., Mouthereau, F., Brichau, S., Crespo-Blanc, A., Gautheron, C., Angrand, P., 2020. Tectono-Stratigraphic and Thermal Evolution of the Western Betic Flysch: Implications for the Geodynamics of South Iberian Margin and Alboran Domain. Tectonics 39. https://doi.org/10.1029/2020tc006093

Dewey, J.F., 1988. Extensional collapse of orogens. Tectonics 7, 1123–1139. https://doi.org/10.1029/tc007i006p01123

Dewey, J.F., Helman, M.L., Knott, S.D., Turco, E., Hutton, D.H.W., 1989. Kinematics of the western Mediterranean. Geological Society, London, Special Publications 45, 265–283. https://doi.org/10.1144/gsl.sp.1989.045.01.15

Diaz, J., Gallart, J., Carbonell, R., 2016. Moho topography beneath the Iberian-Western Mediterranean region mapped from controlled-source and natural seismicity surveys. Tectonophysics 692, 74–85. https://doi.org/10.1016/j.tecto.2016.08.023

Do Couto, D., Gumiaux, C., Augier, R., Lebret, N., Folcher, N., Jouannic, G., Jolivet, L., Suc, J., Gorini, C., 2014. Tectonic inversion of an asymmetric graben: Insights from a combined field and gravity survey in the Sorbas basin. Tectonics 33, 1360–1385. https://doi.org/10.1002/2013tc003458

Duggen, S., Hoernle, K., Bogaard, P. van den, Rüpke, L., Morgan, J.P., 2003. Deep roots of the Messinian salinity crisis. Nature 422, 602–606. https://doi.org/10.1038/nature01553

Duggen, S., Hoernle, K., Bogaard, P. van den, Harris, C., 2004. Magmatic evolution of the Alboran region: The role of subduction in forming the western Mediterranean and causing the Messinian Salinity Crisis. Earth Planet Sc Lett 218, 91–108. https://doi.org/10.1016/s0012-821x(03)00632-0

Duggen, S., Hoernle, K., Klügel, A., Geldmacher, J., Thirlwall, M., Hauff, F., Lowry, D., Oates, N., 2008. Geochemical zonation of the Miocene Alborán Basin volcanism (westernmost Mediterranean): geodynamic implications. Contrib Mineral Petr 156, 577. https://doi.org/10.1007/s00410-008-0302-4

Echeverria, A., Khazaradze, G., Asensio, E., Gárate, J., Dávila, J.M., Suriñach, E., 2013. Crustal deformation in eastern Betics from CuaTeNeo GPS network. Tectonophysics 608, 600–612. https://doi.org/10.1016/j.tecto.2013.08.020

Ercilla, G., Galindo-Zaldívar, J., Estrada, F., Valencia, J., Juan, C., Casas, D., Alonso, B., Comas, M.C., Tendero-Salmerón, V., Casalbore, D., Azpiroz-Zabala, M., Bárcenas, P., Ceramicola, S., Chiocci, F.L., Idárraga-García, J., López-González, N., Mata, P., Palomino, D., Rodríguez-García, J.A., Teixeira, M., Nespereira, J., Vázquez, J.T., Yenes, M., 2022. Understanding the complex geomorphology of a deep sea area affected by continental tectonic indentation: The case of the Gulf of Vera (Western Mediterranean). Geomorphology 402, 108126. https://doi.org/10.1016/j.geomorph.2022.108126

Faccenna, C., Becker, T.W., Auer, L., Billi, A., Boschi, L., Brun, J.P., Capitanio, F.A., Funiciello, F., Horvàth, F., Jolivet, L., Piromallo, C., Royden, L., Rossetti, F., Serpelloni, E., 2014. Mantle dynamics in the Mediterranean. Rev Geophys 52, 283–332. https://doi.org/10.1002/2013rg000444

Fortuin, A.R., Krijgsman, W., 2003. The Messinian of the Nijar Basin (SE Spain): sedimentation, depositional environments and paleogeographic evolution. Sediment Geol 160, 213–242. https://doi.org/10.1016/s0037-0738(02)00377-9

775 Fossen, H., Teyssier, C., Whitney, D.L., 2013. Transtensional folding. Journal of structural geology 56, 89–102.
776   https://doi.org/http://dx.doi.org/10.1016/j.jsg.2013.09.004
777 Fossen, H., Tikoff, B., 1998. Extended models of transpression and transtension, and application to tectonic settings.
778   Geological Society, London, Special Publications 135, 15–33. https://doi.org/10.1144/gsl.sp.1998.135.01.02
779 Frasca, G., Gueydan, F., Brun, J.-P., Monié, P., 2016. Deformation mechanisms in a continental rift up to mantle
780   exhumation. Field evidence from the western Betics, Spain. Mar Petrol Geol 76, 310–328.
781   https://doi.org/10.1016/j.marpetgeo.2016.04.020
782 Galindo-Zaldivar, J., Gonzalez-Lodeiro, F., Jabaloy, A., 2015. Progressive extensional shear structures in a
783   detachment contact in the Western Sierra Nevada (Betic Cordilleras, Spain). Geodin Acta 3, 73–85.
784   https://doi.org/10.1080/09853111.1989.11105175
785 Galindo-Zaldivar, J., Gil, A.J., Borque, M.J., González-Lodeiro, F., Jabaloy, A., Marin-Lechado, C., Ruano, P.,
786   Galdeano, C.S. de, 2003. Active faulting in the internal zones of the central Betic Cordilleras (SE, Spain). J
787   Geodyn 36, 239–250. https://doi.org/10.1016/s0264-3707(03)00049-8
788 Gallais, F., Graindorge, D., Gutscher, M.-A., Klaeschen, D., 2013. Propagation of a lithospheric tear fault (STEP)
789   through the western boundary of the Calabrian accretionary wedge offshore eastern Sicily (Southern Italy).
790   Tectonophysics 602, 141–152. https://doi.org/10.1016/j.tecto.2012.12.026
791 Garcia-Castellanos, D., Villaseñor, A., 2012. Messinian salinity crisis regulated by competing tectonics and erosion
792   at the Gibraltar arc. Nature 480, 359–363. https://doi.org/10.1038/nature10651
793 García-Dueñas, V., Banda, E., Torné, M., Córdoba, D., Group, E.-B.W., 1994. A deep seismic reflection survey
794   across the Betic Chain (southern Spain): first results. Tectonophysics 232, 77–89. https://doi.org/10.1016/0040-
795   1951(94)90077-9
796 Giaconia, F., Booth-Rea, G., Martínez-Martínez, J.M., Azañón, J.M., Pérez-Peña, J.V., Pérez-Romero, J., Villegas,
797   I., 2012. Geomorphic evidence of active tectonics in the Sierra Alhamilla (eastern Betics, SE Spain).
798   Geomorphology 145, 90–106. https://doi.org/10.1016/j.geomorph.2011.12.043
799 Giaconia, F., Booth-Rea, G., Martínez-Martínez, J.M., Azañón, J.M., Pérez-Romero, J., Villegas, I., 2013. Mountain
800   front migration and drainage captures related to fault segment linkage and growth: The Polopos transpressive
801   fault zone (southeastern Betics, SE Spain). J Struct Geol 46, 76–91. https://doi.org/10.1016/j.jsg.2012.10.005
802 Giaconia, F., Booth-Rea, G., Martinez-Martinez, J.M., Azañón, J.M., Storti, F., Artoni, A., 2014. Heterogeneous
803   extension and the role of transfer faults in the development of the southeastern Betic basins (SE Spain).
804   Tectonics 33, 2467–2489. https://doi.org/10.1002/2014tc003681
805 Gomez-Pugnaire, M.T., Fernandez-Soler, J.M., 1987. High-pressure metamorphism in metabasites from the Betic
806   Cordilleras (S.E. Spain) and its evolution during the Alpine orogeny. Contrib Mineral Petr 95, 231–244.
807   https://doi.org/10.1007/bf00381273
808 Gómez de la Peña, L.G. de la, Grevemeyer, I., Kopp, H., Díaz, J., Gallart, J., Booth-Rea, G., Gràcia, E., Ranero,
809   C.R., 2020a. The Lithospheric Structure of the Gibraltar Arc System From Wide-Angle Seismic Data. J Geophys
810   Res Solid Earth 125. https://doi.org/10.1029/2020jb019854
811 Gómez de la Peña, L.G. de la, Ranero, C.R., Gràcia, E., 2018. The Crustal Domains of the Alboran Basin (Western
812   Mediterranean). Tectonics 37, 3352–3377. https://doi.org/10.1029/2017tc004946
813 Gómez de la Peña, L.G. de la, Ranero, C.R., Gràcia, E., Booth-Rea, G., 2020b. The evolution of the westernmost
814   Mediterranean basins. Earth-sci Rev 103445. https://doi.org/10.1016/j.earscirev.2020.103445
815 Govers, R., Wortel, M.J.R., 2005. Lithosphere tearing at STEP faults: response to edges of subduction zones. Earth
816   Planet Sc Lett 236, 505–523. https://doi.org/10.1016/j.epsl.2005.03.022
817 Haq, B., Gorini, C., Baur, J., Moneron, J., & Rubino, J.-L. (2020). Deep Mediterranean's Messinian evaporite giant:
818   How much salt? Global and Planetary Change, 184, 103052.
819   doi:https://doi.org/10.1016/j.gloplacha.2019.103052
820 Haughton, P.D.W., 2000. Evolving turbidite systems on a deforming basin floor, Tabernas, SE Spain.
821   Sedimentology 47, 497–518. https://doi.org/10.1046/j.1365-3091.2000.00293.x
822 Haughton, P.D.W., 1994. Deposits of deflected and ponded turbidity currents, Sorbas Basin, Southeast Spain. J
823   Sediment Res 64, 233–246. https://doi.org/10.1306/d4267d6b-2b26-11d7-8648000102c1865d
824 Heit, B., Mancilla, F. de L., Yuan, X., Morales, J., Stich, D., Martín, R., Molina-Aguilera, A., 2017. Tearing of the
825   mantle lithosphere along the intermediate-depth seismicity zone beneath the Gibraltar Arc: The onset of
826   lithospheric delamination. Geophys Res Lett 44, 4027–4035. https://doi.org/10.1002/2017gl073358
827 Hinsbergen, D.J.J., Vissers, R.L.M., Spakman, W., 2014. Origin and consequences of western Mediterranean
828   subduction, rollback, and slab segmentation. Tectonics 33, 393–419. https://doi.org/10.1002/2013tc003349

Hodgson, D.M., Haughton, P.D.W., 2004. Impact of syndepositional faulting on gravity current behaviour and deep-water stratigraphy: Tabernas-Sorbas Basin, SE Spain. Geological Soc Lond Special Publ 222, 135–158. https://doi.org/10.1144/gsl.sp.2004.222.01.08

Jabaloy-Sánchez, A., Talavera, C., Rodríguez-Peces, M.J., Vázquez-Vílchez, M., Evans, N.J., 2021. U-Pb geochronology of detrital and igneous zircon grains from the Águilas Arc in the Internal Betics (SE Spain): Implications for Carboniferous-Permian paleogeography of Pangea. Gondwana Res 90, 135–158. https://doi.org/10.1016/j.gr.2020.10.013

Janowski, M., Loget, N., Gautheron, C., Barbarand, J., Bellahsen, N., Driessche, J.V. den, Babault, J., Meyer, B., 2017. Neogene exhumation and relief evolution in the eastern Betics (SE Spain): Insights from the Sierra de Gador. Terra Nova 29, 91–97. https://doi.org/10.1111/ter.12252

Johnson, C., Harbury, N., Hurford, A.J., 1997. The role of extension in the Miocene denudation of the Nevado-Filábride Complex, Betic Cordillera (SE Spain). Tectonics 16, 189–204. https://doi.org/10.1029/96tc03289

Jolivet, L., Baudin, T., Calassou, S., Chevrot, S., Ford, M., Issautier, B., Lasseur, E., Masini, E., Manatschal, G., Mouthereau, F., Thinon, I., Vidal, O., 2021a. Geodynamic evolution of a wide plate boundary in the Western Mediterranean, near-field versus far-field interactions. Bsgf - Earth Sci Bulletin 192, 48. https://doi.org/10.1051/bsgf/2021043

Jolivet, L., Faccenna, C., 2000. Mediterranean extension and the Africa-Eurasia collision. Tectonics 19, 1095–1106. https://doi.org/10.1029/2000tc900018

Jolivet, L., Menant, A., Roche, V., Pourhiet, L.L., Maillard, A., Augier, R., Couto, D.D., Gorini, C., Thinon, I., Canva, A., 2021b. Transfer zones in Mediterranean back-arc regions and tear faults. Bsgf - Earth Sci Bulletin 192, 11. https://doi.org/10.1051/bsgf/2021006

Jourdon, A., Kergaravat, C., Duclaux, G., Huguen, C., 2021. Looking beyond kinematics: 3D thermo-mechanical modelling reveals the dynamics of transform margins. Solid Earth 12, 1211–1232. https://doi.org/10.5194/se-12-1211-2021

Juan, C., Ercilla, G., Javier Hernández-Molina, F., Estrada, F., Alonso, B., Casas, D., . . . Ammar, A. (2016). Seismic evidence of current-controlled sedimentation in the Alboran Sea during the Pliocene and Quaternary: Palaeoceanographic implications. Marine Geology, 378, 292-311. doi:https://doi.org/10.1016/j.margeo.2016.01.006

Jurado, M.J., Comas, M.C., 1992. Well log interpretation and seismic character of the cenozoic sequence in the northern Alboran Sea. Geo-Marine Letters 12, 129–136.

Kleverlaan, K., 1989. Neogene history of the Tabernas basin (SE Spain) and its Tortonian submarine fan development. Geologie en Mijnbouw 421–432.

Kleverlaan, K., 1989. Three distinctive feeder-lobe systems within one time slice of the Tortonian Tabernas fan, SE Spain. Sedimentology 36, 25–45. https://doi.org/10.1111/j.1365-3091.1989.tb00818.x

Kleverlaan, K., 1987. Gordo megabed: a possible seismite in a tortonian submarine fan, tabernas basin, province almeria, southeast spain. Sediment Geol 51, 165–180. https://doi.org/10.1016/0037-0738(87)90047-9

Koulali, A., Ouazar, D., Tahayt, A., King, R.W., Vernant, P., Reilinger, R.E., McClusky, S., Mourabit, T., Davila, J.M., Amraoui, N., 2011. New GPS constraints on active deformation along the Africa–Iberia plate boundary. Earth Planet Sc Lett 308, 211–217. https://doi.org/10.1016/j.epsl.2011.05.048

Larouzière, F.D.D., Bolze, J., Bordet, P., Hernandez, J., Montenat, C., d'Estevou, P.O., 1988. The Betic segment of the lithospheric Trans-Alboran shear zone during the Late Miocene. Tectonophysics 152, 41–52. https://doi.org/10.1016/0040-1951(88)90028-5

Lonergan, L., White, N., 1997. Origin of the Betic-Rif mountain belt. Tectonics 16, 504–522. https://doi.org/10.1029/96tc03937

Mancilla, F. de L., Booth-Rea, G., Stich, D., Pérez-Peña, J.V., Morales, J., Azañón, J.M., Martin, R., Giaconia, F., 2015a. Slab rupture and delamination under the Betics and Rif constrained from receiver functions. Tectonophysics. https://doi.org/10.1016/j.tecto.2015.06.028

Mancilla, F. de L., Heit, B., Morales, J., Yuan, X., Stich, D., Molina-Aguilera, A., Azañon, J.M., Martín, R., 2018. A STEP fault in Central Betics, associated with lateral lithospheric tearing at the northern edge of the Gibraltar arc subduction system. Earth Planet Sc Lett 486, 32–40. https://doi.org/10.1016/j.epsl.2018.01.008

Mancilla, F. de L., Stich, D., Morales, J., Martin, R., Diaz, J., Pazos, A., Córdoba, D., Pulgar, J.A., Ibarra, P., Harnafi, M., Gonzalez-Lodeiro, F., 2015b. Crustal thickness and images of the lithospheric discontinuities in the Gibraltar arc and surrounding areas. Geophysical Journal International 203, 1804–1820. https://doi.org/10.1093/gji/ggv390

Martin, J.M., Braga, J.C., Rivas, P., 1989. Coral successions in Upper Tortonian reefs in SE Spain. Lethaia 22, 271–286. https://doi.org/10.1111/j.1502-3931.1989.tb01342.x

Martín, J.M., Braga, J.C., 1994. Messinian events in the Sorbas Basin in southeastern Spain and their implications in the recent history of the Mediterranean. Sediment Geol 90, 257–268. https://doi.org/10.1016/0037-0738(94)90042-6

Martínez-García, P., Comas, M., Lonergan, L., Watts, A.B., 2017. From Extension to Shortening: Tectonic Inversion Distributed in Time and Space in the Alboran Sea, Western Mediterranean. Tectonics 36, 2777–2805. https://doi.org/10.1002/2017tc004489

Martínez-García, P., Soto, J.I., Comas, M., 2011. Recent structures in the Alboran Ridge and Yusuf fault zones based on swath bathymetry and sub-bottom profiling: evidence of active tectonics. Geo-mar Lett 31, 19–36. https://doi.org/10.1007/s00367-010-0212-0

Martínez-Martínez, J.M., Azañón, J.M., 1997. Mode of extensional tectonics in the southeastern Betics (SE Spain): Implications for the tectonic evolution of the peri-Alborán orogenic system. Tectonics 16, 205–225. https://doi.org/10.1029/97tc00157

Martínez-Martínez, J.M., Booth-Rea, G., Azañón, J.M., Torcal, F., 2006. Active transfer fault zone linking a segmented extensional system (Betics, southern Spain): Insight into heterogeneous extension driven by edge delamination. Tectonophysics 422, 159–173. https://doi.org/10.1016/j.tecto.2006.06.001

Martínez-Martínez, J.M., Soto, J.I., Balanyá, J.C., 2002. Orthogonal folding of extensional detachments: Structure and origin of the Sierra Nevada elongated dome (Betics, SE Spain). Tectonics 21, 3-1-3–20. https://doi.org/10.1029/2001tc001283

Martínez-Martos, M., Galindo-Zaldívar, J., Martínez-Moreno, F.J., Calvo-Rayo, R., Galdeano, C.S. de, 2017. Superposition of tectonic structures leading elongated intramontane basin: the Alhabia basin (Internal Zones, Betic Cordillera). Int J Earth Sci 106, 2461–2471. https://doi.org/10.1007/s00531-016-1442-9

Meighan, H.E., Brink, U. ten, Pulliam, J., 2013. Slab tears and intermediate-depth seismicity: slab tears and intermediate seismicity. Geophys Res Lett 40, 4244–4248. https://doi.org/10.1002/grl.50830

Meijninger, B.M.L., Vissers, R.L.M., 2006. Miocene extensional basin development in the Betic Cordillera, SE Spain revealed through analysis of the Alhama de Murcia and Crevillente Faults: Miocene extensional basin development in the Betic Cordillera. Basin Res 18, 547–571. https://doi.org/10.1111/j.1365-2117.2006.00308.x

Montenat, C., D'Estevou, P.O., 1992. Geodynamics of the Eastern Betic late Neogene Basins. A Review. Física de la Tierra 57–75.

Mora, M., 1993. Tectonic and sedimentary analysis of the Huercal-Overa region, South East Spain, Betic Cordillera. University of Oxford, 300 pp.

Moragues, L., Ruano, P., Azañón, J.M., Garrido, C.J., Hidas, K., Booth-Rea, G., 2021. Two Cenozoic Extensional Phases in Mallorca and Their Bearing on the Geodynamic Evolution of the Western Mediterranean. Tectonics 40. https://doi.org/10.1029/2021tc006868.

Mouthereau, F., Angrand, P., Jourdon, A., Ternois, S., Fillon, C., Calassou, S., Chevrot, S., Ford, M., Jolivet, L., Manatschal, G., Masini, E., Thinon, I., Vidal, O., Baudin, T., 2021. Cenozoic mountain building and topographic evolution in Western Europe: impact of billions of years of lithosphere evolution and plate kinematics. Bsgf - Earth Sci Bulletin 192, 56. https://doi.org/10.1051/bsgf/2021040

Mouthereau, F., Filleaudeau, P., Vacherat, A., Pik, R., Lacombe, O., Fellin, M.G., Castelltort, S., Christophoul, F., Masini, E., 2014. Placing limits to shortening evolution in the Pyrenees: Role of margin architecture and implications for the Iberia/Europe convergence. Tectonics 33, 2283–2314. https://doi.org/10.1002/2014tc003663

Neuharth, D., Brune, S., Glerum, A., Morley, C.K., Yuan, X., Braun, J., 2021. Flexural strike-slip basins. Geology. https://doi.org/10.1130/g49351.1

Nocquet, J.-M., 2012. Present-day kinematics of the Mediterranean: A comprehensive overview of GPS results. Tectonophysics 579, 220–242. https://doi.org/10.1016/j.tecto.2012.03.037

Okay, A.I., Tüysüz, O., Kaya, Ş., 2004. From transpression to transtension: changes in morphology and structure around a bend on the North Anatolian Fault in the Marmara region. Tectonophysics 391, 259–282. https://doi.org/10.1016/j.tecto.2004.07.016

Palano, M., González, P.J., Fernández, J., 2015. The Diffuse Plate boundary of Nubia and Iberia in the Western Mediterranean: Crustal deformation evidence for viscous coupling and fragmented lithosphere. Earth and Planetary Science Letters 430, 439–447. https://doi.org/10.1016/j.epsl.2015.08.040

Palano, M., González, P.J., Fernández, J., 2013. Strain and stress fields along the Gibraltar Orogenic Arc: Constraints on active geodynamics. Gondwana Res 23, 1071–1088. https://doi.org/10.1016/j.gr.2012.05.021

Palomeras, I., Thurner, S., Levander, A., Liu, K., Villaseñor, A., Carbonell, R., Harnafi, M., 2014. Finite-frequency Rayleigh wave tomography of the western Mediterranean: Mapping its lithospheric structure. Geochemistry, Geophysics, Geosystems 15, 140–160. https://doi.org/10.1002/2013gc004861

Pedrera, A., Galindo-Zaldívar, J., Galdeano, C.S. de, López-Garrido, Á.C., 2007. Fold and fault interactions during the development of an elongated narrow basin: The Almanzora Neogene-Quaternary Corridor (SE Betic Cordillera, Spain): FOLD AND FAULT INTERACTIONS. Tectonics 26, n/a-n/a. https://doi.org/10.1029/2007tc002138

Pedrera, A., Galindo-Zaldívar, J., Ruíz-Constán, A., Duque, C., Marín-Lechado, C., Serrano, I., 2009. Recent large fold nucleation in the upper crust: Insight from gravity, magnetic, magnetotelluric and seismicity data (Sierra de Los Filabres–Sierra de Las Estancias, Internal Zones, Betic Cordillera). Tectonophysics 463, 145–160. https://doi.org/10.1016/j.tecto.2008.09.037

Pedrera, A., Galindo-Zaldívar, J., Tello, A., Marín-Lechado, C., 2010. Intramontane basin development related to contractional and extensional structure interaction at the termination of a major sinistral fault: The Huércal-Overa Basin (Eastern Betic Cordillera). J Geodyn 49, 271–286. https://doi.org/10.1016/j.jog.2010.01.008

Pickering, K.T., Hodgson, D.M., Platzman, E., Clark, J.D., Stephens, C., 2001. A New Type of Bedform Produced by Backfilling Processes in a Submarine Channel, Late Miocene, Tabernas-Sorbas Basin, SE Spain. J Sediment Res 71, 692–704. https://doi.org/10.1306/2dc40960-0e47-11d7-8643000102c1865d

Pindell, J.L., Kennan, L., 2009. Tectonic evolution of the Gulf of Mexico, Caribbean and northern South America in the mantle reference frame: an update. Geological Soc Lond Special Publ 328, 1–55. https://doi.org/10.1144/sp328.1

Platt, J.P., Behr, W.M., Johanesen, K., Williams, J.R., 2013. The Betic-Rif Arc and Its Orogenic Hinterland: A Review. Annual Review of Earth and Planetary Sciences 41, 313–357. https://doi.org/10.1146/annurev-earth-050212-123951

Platt, J.P., Kelley, S.P., Carter, A., Orozco, M., 2005. Timing of tectonic events in the Alpujárride Complex, Betic Cordillera, southern Spain. J Geol Soc London 162, 451–462. https://doi.org/10.1144/0016-764903-039

Platt, J.P., Anczkiewicz, R., Soto, J.-I., Kelley, S.P., Thirlwall, M., 2006. Early Miocene continental subduction and rapid exhumation in the western Mediterranean. Geology 34, 981–984. https://doi.org/10.1130/g22801a.1

Platt, J.P., Vissers, R.L.M., 1989. Extensional collapse of thickened continental lithosphere: A working hypothesis for the Alboran Sea and Gibraltar arc. Geology 17, 540–543. https://doi.org/10.1130/0091-7613(1989)017<0540:ecotcl>2.3.co;2

Platt, J.P., Whitehouse, M.J., 1999. Early Miocene high-temperature metamorphism and rapid exhumation in the Betic Cordillera (Spain): evidence from U–Pb zircon ages. Earth and Planetary Science Letters 171, 591–605.

Platzman, E.S., 1992. Paleomagnetic rotations and the kinematics of the Gibraltar arc. Geology 20, 311–314. https://doi.org/10.1130/0091-7613(1992)020<0311:pratko>2.3.co;2

Poisson, A., Guezou, J.C., Ozturk, A., Inan, S., Temiz, H., Gürsöy, H., Kavak, K.S., ÖZDEN, S., 1996. Tectonic Setting and Evolution of the Sivas Basin, Central Anatolia, Turkey. International Geology Review 38, 838–853. https://doi.org/10.1080/00206819709465366

Poisson, A.M., Morel, J.L., Andrieux, J., Coulon, M., Wernli, R., Guernet, C., 1999. The origin and development of neogene basins in the SE Betic Cordillera (SE Spain): a case study of the Tabernas-Sorbas and Huercal Overa basins. J Petrol Geol 22, 97–114. https://doi.org/10.1111/j.1747-5457.1999.tb00461.x

Pourhiet, L.L., Huet, B., May, D.A., Labrousse, L., Jolivet, L., 2012. Kinematic interpretation of the 3D shapes of metamorphic core complexes: 3D SHAPES OF MCCs. Geochem Geophys Geosystems 13. https://doi.org/10.1029/2012gc004271

Pownall, J.M., Hall, R., Watkinson, I.M., 2013. Extreme extension across Seram and Ambon, eastern Indonesia: evidence for Banda slab rollback. Solid Earth 4, 277–314. https://doi.org/10.5194/se-4-277-2013

Rat, J., Mouthereau, F., Brichau, S., Crémades, A., Bernet, M., Balvay, M., Ganne, J., Lahfid, A., Gautheron, C., 2019. Tectonothermal Evolution of the Cameros Basin: Implications for Tectonics of North Iberia. Tectonics 38, 440–469. https://doi.org/10.1029/2018tc005294

Rat, J., Mouthereau, F., Brichau, S., Vacherat, A., Fillon, C., Gautheron, C., 2022. Timing and distribution of exhumation in the Ebro basin reveal a plate-scale 10 Ma geodynamic event. Global Planet Change 103973. https://doi.org/10.1016/j.gloplacha.2022.103973

Reicherter, K., Hübscher, C., 2006. Evidence for a seafloor rupture of the Carboneras Fault Zone (southern Spain): Relation to the 1522 Almería earthquake? J Seismol 11, 15–26. https://doi.org/10.1007/s10950-006-9024-0

Reinhardt, L.J., Dempster, T.J., Shroder, J.F., Persano, C., 2007. Tectonic denudation and topographic development in the Spanish Sierra Nevada. Tectonics 26, n/a-n/a. https://doi.org/10.1029/2006tc001954

Richards, J.P., 2009. Postsubduction porphyry Cu-Au and epithermal Au deposits: Products of remelting of subduction-modified lithosphere. Geology 37, 247–250. https://doi.org/10.1130/g25451a.1

Riding, R., Braga, J.C., Martín, J.M., Sánchez-Almazo, I.M., 1998. Mediterranean Messinian Salinity Crisis: constraints from a coeval marginal basin, Sorbas, southeastern Spain. Mar Geol 146, 1–20. https://doi.org/10.1016/s0025-3227(97)00136-9

Rodríguez-Fernández, J., Azor, A., Azañón, J.M., 2012. Tectonics of Sedimentary Basins 461–479. https://doi.org/10.1002/9781444347166.ch23

Romagny, A., Jolivet, L., Menant, A., Bessière, E., Maillard, A., Canva, A., Gorini, C., Augier, R., 2020. Detailed tectonic reconstructions of the Western Mediterranean region for the last 35 Ma, insights on driving mechanisms. Bsgf - Earth Sci Bulletin 191, 37. https://doi.org/10.1051/bsgf/2020040

Rosenbaum, G., Lister, G.S., Duboz, C., 2002. Relative motions of Africa, Iberia and Europe during Alpine orogeny. Tectonophysics 359, 117–129. https://doi.org/10.1016/s0040-1951(02)00442-0

Sanz de Galdeano, C.S., Vera, J.A., 1992. Stratigraphic record and palaeogeographical context of the Neogene basins in the Betic Cordillera, Spain. Basin Res 4, 21–36. https://doi.org/10.1111/j.1365-2117.1992.tb00040.x

Sanz de Galdeano, C.S.D., Rodriguez-Fernandez, J., Lopez-Garrido, A.C., 1985. A strike-slip fault corridor within the Alpujarra Mountains (Betic Cordilleras, Spain). Geol Rundsch 74, 641–655. https://doi.org/10.1007/bf01821218

Sanz de Galdeano, C.S. de, Alfaro, P., 2004. Tectonic significance of the present relief of the Betic Cordillera. Geomorphology 63, 175–190. https://doi.org/10.1016/j.geomorph.2004.04.002

Scotney, P., Burgess, R., Rutter, E.H., 2000. 40Ar/39Ar age of the Cabo de Gata volcanic series and displacements on the Carboneras fault zone, SE Spain. J Geol Soc London 157, 1003–1008. https://doi.org/10.1144/jgs.157.5.1003

Sosson, M., Morrillon, A.-C., Bourgois, J., Féraud, G., Poupeau, G., Saint-Marc, P., 1998. Late exhumation stages of the Alpujarride Complex (western Betic Cordilleras, Spain): new thermochronological and structural data on Los Reales and Ojen nappes. Tectonophysics 285, 253–273. https://doi.org/10.1016/s0040-1951(97)00274-6

Spakman, W., Wortel, R., 2004. The TRANSMED Atlas. The Mediterranean Region from Crust to Mantle 31–52. https://doi.org/10.1007/978-3-642-18919-7_2

Spakman, W., Chertova, M.V., Berg, A. van Hinsbergen, D.J.J., 2018. Puzzling features of western Mediterranean tectonics explained by slab dragging. Nat Geosci 11. https://doi.org/10.1038/s41561-018-0066-z

Stich, D., Serpelloni, E., Mancilla, F. de L., Morales, J., 2006. Kinematics of the Iberia–Maghreb plate contact from seismic moment tensors and GPS observations. Tectonophysics 426, 295–317. https://doi.org/10.1016/j.tecto.2006.08.004

Teyssier, C., Tikoff, B., 1998. Strike-slip partitioned transpression of the San Andreas fault system: a lithospheric-scale approach. Geological Soc Lond Special Publ 135, 143–158. https://doi.org/10.1144/gsl.sp.1998.135.01.10

Vacherat, A., Mouthereau, F., Pik, R., Bellahsen, N., Gautheron, C., Bernet, M., Daudet, M., Balansa, J., Tibari, B., Jamme, R.P., Radal, J., 2016. Rift-to-collision transition recorded by tectonothermal evolution of the northern Pyrenees. Tectonics 35, 907–933. https://doi.org/10.1002/2015tc004016

van Hinsbergen, D.J.J., Vissers, R.L.M., Spakman, W., 2014. Origin and consequences of western Mediterranean subduction, rollback, and slab segmentation. Tectonics 33, 393–419. https://doi.org/10.1002/2013tc003349

Vázquez, M., Jabaloy, A., Barbero, L., Stuart, F.M., 2011. Deciphering tectonic- and erosion-driven exhumation of the Nevado-Filábride Complex (Betic Cordillera, Southern Spain) by low temperature thermochronology: Deciphering tectonic- and erosion-driven exhumation. Terra Nova 23, 257–263. https://doi.org/10.1111/j.1365-3121.2011.01007.x

Vergés, J., Fernàndez, M., 2012. Tethys–Atlantic interaction along the Iberia–Africa plate boundary: The Betic–Rif orogenic system. Tectonophysics 579, 144–172. https://doi.org/10.1016/j.tecto.2012.08.032

Vernant, P., Fadil, A., Mourabit, T., Ouazar, D., Koulali, A., Davila, J.M., Garate, J., McClusky, S., Reilinger, R., 2010. Geodetic constraints on active tectonics of the Western Mediterranean: Implications for the kinematics and dynamics of the Nubia-Eurasia plate boundary zone. J Geodyn 49, 123–129. https://doi.org/10.1016/j.jog.2009.10.007

Villasenor, A., Chevrot, S., Harnafi, M., Gallart, J., Pazos, A., Serrano, I., Córdoba, D., Pulgar, J.A., Ibarra, P., 2015. Subduction and volcanism in the Iberia–North Africa collision zone from tomographic images of the upper mantle. Tectonophysics. https://doi.org/10.1016/j.tecto.2015.08.042

Waldner, M., Bellahsen, N., Mouthereau, F., Bernet, M., Pik, R., Rosenberg, C.L., Balvay, M., 2021. Central Pyrenees Mountain Building: Constraints From New LT Thermochronological Data From the Axial Zone. Tectonics 40. https://doi.org/10.1029/2020tc006614

Weijermars, R., Roep, Th.B., Eeckhout, B.V. den, Postma, G., Kleverlaan, K., 1985. Uplift history of a Betic fold nappe inferred from Neogene-Quaternary sedimentation and tectonics (in the Sierra Alhamilla and Almeria, Sorbas and Tabernas Basins of the Betic Cordilleras, SE Spain). Geologie en Mijnbouw 397–411.

1050   Zeck, H.P., Monié, P., Villa, I.M., Hansen, B.T., 1992. Very high rates of cooling and uplift in the Alpine belt of the
1051   Betic Cordilleras, southern Spain. Geology 20, 79. https://doi.org/10.1130/0091-
1052   7613(1992)020<0079:vhroca>2.3.co;2
1053